Gastroenterology 2021;161:968–981

BASIC AND TRANSLATIONAL—LIVER

Associations Among Adipose Tissue Immunology, Inflammation, Exosomes and Insulin Sensitivity in People With Obesity and Nonalcoholic Fatty Liver Disease

Anja Fuchs,[1] Dmitri Samovski,[2] Gordon I. Smith,[2] Vincenza Cifarelli,[2] Sarah S. Farabi,[2] Jun Yoshino,[2] Terri Pietka,[2] Shin-Wen Chang,[1] Sarbani Ghosh,[1] Terence M. Myckatyn,[1] and Samuel Klein[2]

[1]Department of Surgery, Washington University School of Medicine, St. Louis, Missouri; and [2]Center for Human Nutrition, Washington University School of Medicine, St. Louis, Missouri

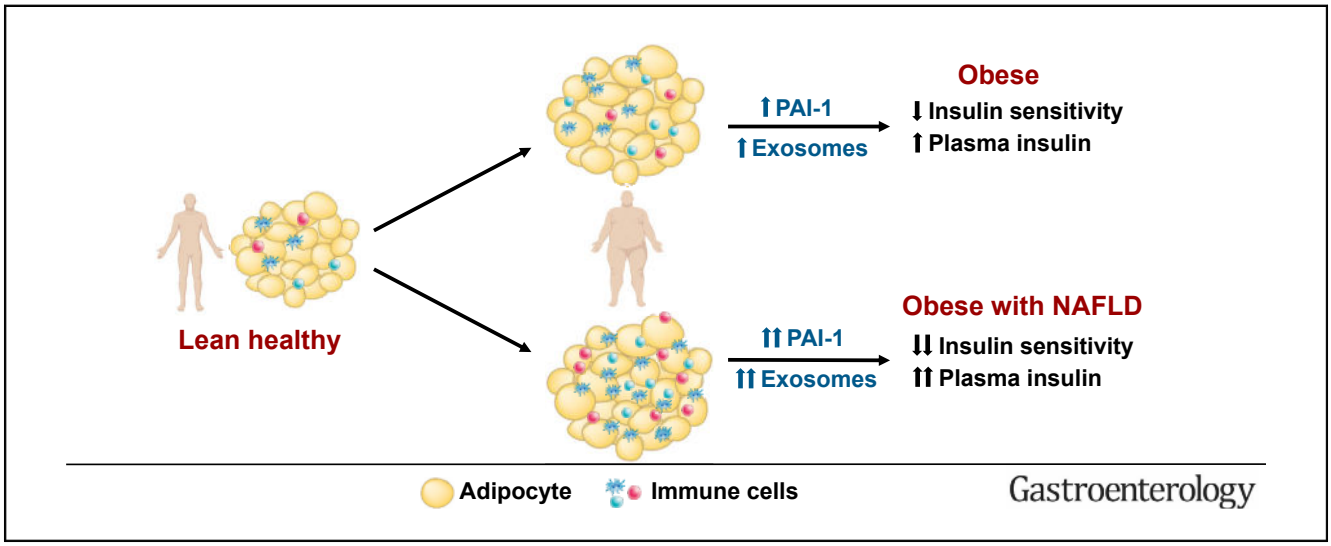

BACKGROUND AND AIMS: Insulin resistance is a key factor in the pathogenesis of nonalcoholic fatty liver disease (NAFLD). We evaluated the importance of subcutaneous abdominal adipose tissue (SAAT) inflammation and both plasma and SAAT–derived exosomes in regulating insulin sensitivity in people with obesity and NAFLD. **METHODS:** Adipose tissue inflammation (macrophage and T-cell content and expression of proinflammatory cytokines), liver and whole-body insulin sensitivity (assessed using a hyperinsulinemic-euglycemic clamp and glucose tracer infusion), and 24-hour serial plasma cytokine concentrations were evaluated in 3 groups stratified by adiposity and intrahepatic triglyceride (IHTG) content: (1) lean with normal IHTG content (LEAN; N = 14); (2) obese with normal IHTG content (OB-NL; N = 28); and (3) obese with NAFLD (OB-NAFLD; N = 28). The effect of plasma and SAAT–derived exosomes on insulin-stimulated Akt phosphorylation in human skeletal muscle myotubes and mouse primary hepatocytes was assessed in a subset of participants. **RESULTS:** Proinflammatory macrophages, proinflammatory CD4 and CD8 T-cell populations, and gene expression of several cytokines in SAAT were greater in the OB-NAFLD than the OB-NL and LEAN groups. However, with the exception of PAI-1, which was greater in the OB-NAFLD than the LEAN and OB-NL groups, 24-hour plasma cytokine concentration areas-under-the-curve were not different between groups. The percentage of proinflammatory macrophages and plasma PAI-1 concentration areas-under-the-curve were inversely correlated with both hepatic and whole-body insulin sensitivity. Compared with exosomes from OB-NL participants, plasma and SAAT–derived exosomes from the OB-NAFLD group decreased insulin signaling in myotubes and hepatocytes. **CONCLUSIONS:** Systemic insulin resistance in people with obesity and NAFLD is associated with increased plasma PAI-1 concentrations and both plasma and SAAT-derived exosomes. ClinicalTrials.gov number: NCT02706262 (https://clinicaltrials.gov/ct2/show/NCT02706262).

Keywords: Macrophages; T Cells; Cytokines; Insulin Resistance; PAI-1.

Hepatic steatosis is the hallmark feature of nonalcoholic fatty liver disease (NAFLD) and occurs commonly in people with obesity.[1] Obesity-induced insulin resistance is involved in the pathogenesis of NAFLD and hepatic steatosis is unlikely to occur in people with obesity who do not have significant insulin resistance.[2,3] Even people with a genetic variant of the patatin-like phospholipase domain-containing 3 gene, which markedly increases the risk of NAFLD, are unlikely to develop hepatic steatosis in the absence of obesity and concomitant insulin resistance.[4] The therapeutic effect of pharmacologic agents that increase insulin sensitivity on intrahepatic triglyceride (IHTG) content and other histologic features of NAFLD provides further support for the role of insulin resistance in the pathogenesis of NAFLD.[5,6] These findings underscore the importance of understanding the underlying mechanism(s) responsible for insulin resistance in people with obesity and NAFLD.

It has been proposed that an increase in adipose tissue (AT) proinflammatory immune cells and inflammation, which increases the secretion of inflammatory cytokines from AT into the bloodstream, is an important cause of obesity-induced insulin resistance in people.[7] In rodent models, obesity and insulin resistance are associated with increased adipose tissue macrophage (ATM) and T-cell content and AT gene expression of proinflammatory cytokines.[8] Experimentally decreasing or completely eliminating tumor necrosis factor (TNF)-α signaling[9,10] or shifting the T-cell pool toward higher proportions of anti-inflammatory cells[11,12] promotes glucose tolerance and improves insulin sensitivity. However, the importance of AT inflammation in causing insulin resistance in people with obesity is not clear because of conflicting data among studies, which have found increases in proinflammatory macrophages and CD4 T cells in subcutaneous abdominal AT (SAAT) obtained from people with obesity who were considered to be insulin-resistant compared with those who were insulin-sensitive,[13–15] whereas other studies found no differences between insulin-sensitive and insulin-resistant groups.[16–18] The reason(s) for the discrepant findings among studies could be related to differences in the methods used to assess AT inflammation and immune cell content and differences in the criteria used to define insulin-sensitive and insulin-resistant cohorts.

Exosomes are membrane-bound extracellular vesicles that are produced by most cells in the body and provide a mechanism for interorgan communication by delivering microRNAs (miRNAs), bioactive lipids, and regulatory proteins from one cell to another.[19] Data from studies conducted in rodent models have shown exosomes derived from AT explants[20] and ATMs[21,22] can regulate systemic insulin action mediated by the transfer of specific miRNAs.[21,22] AT is the major source of miRNAs in circulating exosomes; AT-specific knockout of the miRNA-producing enzyme Dicer in mice causes more than a 4-fold reduction in circulating exosomal miRNAs.[23] Therefore, it is possible that AT-derived exosomes contribute to systemic insulin resistance in people with obesity and NAFLD.

WHAT YOU NEED TO KNOW

BACKGROUND AND CONTEXT

Insulin resistance is a common feature of obesity and is a critical factor in the pathogenesis of nonalcoholic fatty liver disease (NAFLD).

NEW FINDINGS

Adipose tissue proinflammatory immune cells and markers of inflammation are increased in people with obesity and NAFLD compared with people with obesity and normal intrahepatic triglyceride content. Adipose tissue–derived PAI-1 and exosomes are associated with insulin resistance in people with obesity and NAFLD.

LIMITATIONS

This clinical study demonstrates a link between insulin resistance and both adipose tissue–derived PAI-1 and exosomes in people with NAFLD, but is unable to determine whether this relationship is causal.

IMPACT

Our findings support the potential importance of alterations in adipose tissue biology in the pathogenesis of insulin resistance in people with obesity and NAFLD.

In the present study, we assessed the potential importance of AT inflammation, systemic mediators of AT inflammation, and exosomes in the pathogenesis of insulin resistance in people with obesity and NAFLD. We evaluated the composition of AT resident immune cells, the AT expression of genes that encode for cytokines and markers of macrophages and T cells, plasma cytokine concentrations obtained serially for 24 hours, and the effect of exosomes isolated from plasma and AT on insulin action ex vivo in 3 distinct groups of participants who were separated based on adiposity, oral glucose tolerance, and IHTG content: (1) healthy lean (LEAN, defined as body mass index [BMI] 18.5–24.9 kg/m^2, normal oral glucose tolerance test [OGTT], HbA1c, and IHTG content); (2) obese with normal IHTG content (OB-NL; defined as BMI 30–49.9 kg/m^2, normal OGTT, HbA1c, and IHTG content); and (3) obese with NAFLD (OB-NAFLD; defined as BMI 30–49.9 kg/m^2, abnormal OGTT and/or HbA1c, and hepatic steatosis). We hypothesized that: (1) AT proinflammatory immune cell

Abbreviations used in this paper: **AT, adipose tissue; ATM, adipose tissue macrophage; AUC, area under the curve; BMI, body mass index; IAAT, intra-abdominal adipose tissue; IFN, interferon; IHTG, intrahepatic triglyceride; IL, interleukin; LEAN, lean with normal intrahepatic triglyceride content; miRNA, microRNA; NAFLD, nonalcoholic fatty liver disease; OB-NL, obese with normal intrahepatic triglyceride content; OB-NAFLD, obese with NAFLD; OGTT, oral glucose tolerance test; SAAT, subcutaneous abdominal adipose tissue; TG, triglyceride; TNF, tumor necrosis factor.**

Most current article

0016-5085/$36.00
https://doi.org/10.1053/j.gastro.2021.05.008

subsets, AT gene expression of cytokines, and plasma cytokine concentrations would progressively increase from LEAN to the OB-NL group to the OB-NAFLD group; (2) AT proinflammatory macrophages and T cells would be negatively associated with hepatic and skeletal muscle insulin sensitivity (assessed using the hyperinsulinemic-euglycemic clamp procedure in conjunction with stable isotopically labeled glucose tracer infusion); and (3) exosomes derived from plasma and SAAT obtained from OB-NAFLD participants, but not LEAN or OB-NL participants, would impair insulin signaling in human myotubes and mouse hepatocytes.

Methods

Study Participants

Seventy men and women participated in this study (14 men and 56 women; age 38 ± 1 years old) from May 2016–April 2020, which was conducted in the Clinical Translational Research Unit at Washington University School of Medicine in St. Louis, MO (Supplementary Figure 1). Some of the data reported here were obtained from a subset of subjects as part of their participation in another study.[24] Written informed consent was obtained from all subjects before their participation in this study, which was approved by the Institutional Review Board at Washington University School of Medicine in St. Louis, MO.

All participants completed a comprehensive screening evaluation, including a medical history and physical examination, standard blood tests, HbA1c, an OGTT, and assessment of IHTG content using magnetic resonance imaging to determine eligibility for each study cohort based on the following inclusion criteria: (1) LEAN had BMI 18.5–24.9 kg/m^2, IHTG content ≤4%, serum triglyceride (TG) concentration <150 mg/dL, fasting plasma glucose concentration <100 mg/dL, 2-hour OGTT plasma glucose concentration ≤140 mg/dL, and HbA1c ≤5.6%; (2) OB-NL had BMI 30.0–49.9 kg/m^2, IHTG content ≤4%, serum TG concentration <150 mg/dL, fasting plasma glucose concentration <100 mg/dL, 2-hour OGTT plasma glucose concentration ≤140 mg/dL, and HbA1c ≤5.6%; and (3) OB-NAFLD had BMI 30–49.9 kg/m^2, IHTG content ≥5.6%, and HbA1c 5.7%–6.4% or fasting plasma glucose concentration 100–125 mg/dL or 2-hour OGTT plasma glucose concentration 140–199 mg/dL. Potential participants who had a history of diabetes or liver disease other than NAFLD, were taking medications that could affect metabolism, or consumed excessive amounts of alcohol (>21 U/wk for men and >14 U/wk for women) were excluded.

We evaluated whether plasma and SAAT–derived exosomes from the OB-NAFLD group can induce insulin resistance in human skeletal muscle myotubes and mouse hepatocytes by studying a subset of participants in whom there was an adequate amount of stored plasma to isolate exosomes (9 LEAN, 8 OB-NL, and 7 OB-NAFLD) and by obtaining fresh SAAT for exosome isolation in an additional 9 OB-NL and 6 OB-NAFLD participants (participant characteristics are provided in Supplementary Tables 1 and 2).

Body Composition Analyses

Total body fat and fat-free mass were determined using dual-energy X-ray absorptiometry. Intra-abdominal AT (IAAT) and SAAT volumes and IHTG content were assessed using magnetic resonance imaging.

Metabolic Testing

Serial 24-hour plasma cytokine concentrations and hyperinsulinemic-euglycemic clamp procedure. Subjects were admitted to the Clinical Translational Research Unit at 1700 hours for ∼48 hours and consumed a standard meal between 1800 hours and 1900 hours. At 0630 hours the next morning (day 2), a catheter was inserted into an antecubital vein and blood samples were obtained every hour from 0700 hours to 2300 hours and at 0500 hours and 0700 hours the following day (day 3). Meals were provided at 0700 hours, 1300 hours, and 1900 hours. Each meal contained one third of the participant's energy requirements and were composed of 50% carbohydrate, 35% fat, and 15% protein. A hyperinsulinemic-euglycemic clamp procedure, in conjunction with stable isotopically labeled glucose tracer infusion, was then conducted to assess hepatic and skeletal muscle insulin sensitivity. Subcutaneous abdominal AT was obtained from the periumbilical area during the basal period of the clamp procedure. Details of all procedures are provided in the Supplementary materials.

Sample Analysis and Calculations

Plasma glucose concentration was determined using an automated glucose analyzer. Plasma insulin, HbA1c, liver enzymes, and lipid profile were measured in the Washington University Core Laboratory for Clinical Studies. Plasma cytokine concentrations were determined using a Luminex 200 analyzer (Luminex Corp., Austin, TX). Plasma 24-hour cytokine concentration area under the curve (AUC) was calculated using the trapezoidal method[25] to provide a comprehensive assessment of daily plasma cytokine levels. Hepatic and skeletal muscle insulin sensitivity were determined as described in the Supplementary material.

Exosomes were isolated from plasma and SAAT explant cultures and incubated with human skeletal muscle myotubes and mouse primary hepatocytes to assess insulin-stimulated phosphorylation of serine 473 of Akt as described in the Supplementary materials. The studies in mice were approved by the Washington University Animal Studies Committee. Standard methods were used for AT RNA sequencing, AT stromal vascular fraction isolation, in vitro stimulation and intracellular cytokine staining of isolated AT immune cells, flow cytometry, and mass cytometry, as described in the Supplementary materials.

Statistical Analysis

One-way analysis of variance was used to compare subject characteristics and outcomes measured at a single time point among LEAN, OB-NL, and OB-NAFLD groups with Fisher least significant difference post-hoc procedure used to identify significant mean differences where appropriate. Polynomial contrasts were performed for selected variables to describe the linear trend from the LEAN group to the OB-NL group to the OB-NAFLD group. Plasma cytokine profiles during 24 hours were analyzed using linear mixed model analysis with time and group as fixed factors. Outliers in plasma cytokine concentrations in the 24-hour profiles (defined as >3 standard deviations

from the mean) were winsorized, and those values were adjusted to match the next less extreme value[26]; this occurred in <2% of values for each cytokine. Relationships among insulin sensitivity and the proportion of proinflammatory and anti-inflammatory macrophages and proinflammatory T cells were evaluated using linear and nonlinear regression analysis with the best fit to the data reported. Data are reported as means ± SEM unless otherwise noted. Statistical analyses were performed using SPSS (version 25, IBM, Armonk, NY).

Based on the previously reported interindividual variability in total macrophage number per gram of SAAT and the proportion of total SAAT macrophages that are proinflammatory,[27] we estimated that 28 subjects per group would be needed to detect differences in total macrophage number of 10,900 cells/g SAAT and percentage of proinflammatory macrophages of 12.3% between the OB-NL and OB-NAFLD groups using a 2-sided test with ≥90% power and an α value of <.05.

Results

Body Composition and Metabolic Characteristics of LEAN, OB-NL, and OB-NAFLD Groups

BMI, percentage of body fat, and SAAT volume were not different in the OB-NL and OB-NAFLD groups, but IAAT volume and IHTG content were much greater in the OB-NAFLD than in the OB-NL group (Table 1). Although IAAT volumes were greater in the OB-NL than the LEAN group, there was no difference in IHTG content between groups. Fasting plasma glucose, plasma glucose 2 hours after glucose ingestion, plasma TG, and HbA1c were higher in the OB-NAFLD group than in both the OB-NL and LEAN groups, without any differences between the 2 groups with normal IHTG content (Table 1). Plasma alanine aminotransferase and aspartate aminotransferase concentrations were higher in the OB-NAFLD than in the OB-NL group (Table 1). Fasting plasma insulin concentration progressively increased and both hepatic insulin sensitivity (assessed as the Hepatic Insulin Sensitivity Index, which is the reciprocal of the product of basal endogenous glucose production rate and basal plasma insulin concentration) and skeletal muscle insulin sensitivity (assessed as the glucose disposal rate relative to plasma insulin concentration during the hyperinsulinemic-euglycemic clamp procedure) progressively decreased from the LEAN group to the OB-NL group to the OB-NAFLD group (Table 1). Hepatic and skeletal muscle insulin sensitivity were lower in the OB-NL group than the LEAN group, although both groups had normal IHTG content.

Proinflammatory Macrophages are Increased in SAAT in People With Obesity

To help characterize ATMs as either proinflammatory ("M1-like") or anti-inflammatory ("M2-like") subsets, we used mass cytometry to assess the expression of macrophage-related proteins on the surface of stromal vascular fraction cells from 4 participants (2 LEAN and 2 OB-NAFLD). Consistent with a previous study,[13] ATMs were classified into 2 subsets: (1) $CD206^+$ $CD11c^-$ macrophages; and (2) $CD206^+$ $CD11c^+$ macrophages (Supplementary Figure 2*A*). We also identified a third subset of CD64 positive cells, but did not categorize those cells as macrophages because they either did not express or expressed very low levels of markers that are characteristic of known macrophage subsets (CD206, HLA-DR, CD9, and CD163) (Supplementary Figure 2*B*) and have been characterized as monocytes, not macrophages.[13] The $CD206^+$ $CD11c^-$ subset tended to express higher levels of markers associated with anti-inflammatory macrophages (CD206 and CD163), whereas the $CD206^+$ $CD11c^+$ subset tended to express higher levels of the costimulatory marker CD86 and contained a population of $CD9^+$ cells, which is a marker associated with crown-like structure macrophages.[28] Within each macrophage subset, cells from LEAN and OB-NAFLD participants tended to express similar levels of the other surface markers. Based on this analysis, we defined $CD206^+$ $CD11c^-$ ATMs as being anti-inflammatory (M2-like) and $CD206^+$ $CD11c^+$ ATMs as being proinflammatory (M1-like), and used these markers for all subsequent flow cytometric analyses. Nonetheless, it is likely that the M1-like and M2-like ATM subsets comprise heterogeneous mixtures of cells with both M1-like and M2-like features.

The number of total, M1-like, and M2-like macrophages increased progressively from the LEAN group to the OB-NL group to the OB-NAFLD group, and the number of total macrophages and M1-like macrophages were greater in the OB-NAFLD than the OB-NL group (Figure 1*A*). In addition, the proportion of total macrophages that were M1-like progressively increased, whereas the proportion that were M2-like progressively decreased, from the LEAN group to the OB-NL group to the OB-NAFLD group, and the mean values in the OB-NAFLD group were significantly different than the mean values in the OB-NL group (Figure 1*B*, Supplementary Figure 3*A*). Accordingly, the ratio of M1-like to M2-like macrophages increased progressively from the LEAN group to the OB-NL group to the OB-NAFLD group. The proportion of M1-like macrophages and the M1-like to M2-like ratio among all subjects were negatively associated, whereas the proportion of M2-like macrophages was positively associated with both hepatic (Figure 1*C*) and muscle (Figure 1*D*) insulin sensitivity. Adipose tissue monocytes, which can differentiate into macrophages, were not different between the LEAN, OB-NL, and OB-NAFLD groups (Supplementary Figure 4). However, the number of classical dendritic cells, which are another myeloid cell subset that has important functions in initiating immune responses via antigen presentation to T cells, was lower in the LEAN group than the OB-NL and OB-NAFLD groups, without a difference between the 2 obese groups (Supplementary Figure 4).

Increase in Memory T Cells in AT From OB-NAFLD Participants

There were no differences in the total number of cells within T-cell subsets (CD4 T cells, CD8 T cells, naïve CD4 T cells, memory CD4 T cells, naïve CD8 T cells, and memory CD8 T cells) or natural killer cells per gram of SAAT among the LEAN, OB-NL, and OB-NAFLD groups (Figure 2*A*, Supplementary Figure 4). However, when analyzed as

Table 1. Body Composition and Metabolic Characteristics of Participants

	LEAN (N = 14)	OB-NL (N = 28)	OB-NAFLD (N = 28)
Age (*y*)	36 ± 2	36 ± 1	42 ± 2[b]
Body mass index (*kg/m²*)	22.9 ± 0.4	37.7 ± 0.9[a]	39.2 ± 0.9[a]
Body fat (%)	29.4 ± 1.6	48.0 ± 1.1[a]	48.6 ± 0.8[a]
IHTG content (%)	1.8 ± 0.2	2.4 ± 0.2	17.5 ± 1.7[a,b]
IAAT volume (*cm³*)	457 ± 53	938 ± 89[a]	1928 ± 141[a,b]
SAAT volume (*cm³*)	963 ± 94	3701 ± 181[a]	3798 ± 237[a]
Alanine aminotransferase (*U/L*)	15 ± 2	16 ± 1	37 ± 8[a,b]
Aspartate aminotransferase (*U/L*)	19 ± 2	17 ± 1	26 ± 3[b]
Fasting TG (*mg/dL*)	72 ± 8	69 ± 4	135 ± 8[a,b]
HbA1c (%)	5.0 ± 0.1	5.1 ± 0.1	5.5 ± 0.1[a,b]
Fasting insulin (*μU/mL*)	5.2 ± 0.5	12.3 ± 1.3[a]	27.8 ± 3.0[a,b]
Fasting glucose (*mg/dL*)	86 ± 1	88 ± 1	97 ± 2[a,b]
Glucose at 2 h of OGTT (*mg/dL*)	98 ± 5	107 ± 3	158 ± 4[a,b]
HISI (*1000/[μmol/kg FFM/min] x [μU/mL]*)	10.9 ± 1.2	5.6 ± 0.4[a]	2.9 ± 0.2[a,b]
Glucose Rd/insulin (*nmol/kg FFM/min)/(μU/mL*)	683 ± 65	383 ± 33[a]	206 ± 17[a,b]

NOTE. Data are expressed as mean ± SEM.
[a]$P \leq .05$ value significantly different from the corresponding value in the LEAN group.
[b]$P \leq .05$ value significantly different from the corresponding value in the OB-NL group.

proportions within T-cell subgroups, the percentage of memory CD4 and CD8 T cells were greater in the OB-NAFLD than in the OB-NL and LEAN groups, without a difference between the LEAN and OB-NL groups, whereas the percentage of naïve CD4 and CD8 T cells were lower in the OB-NAFLD than in the OB-NL and LEAN groups (Figure 2*A*, Supplementary Figure 3*B*). Among memory CD4 T cells, we found progressive increases in the number of Th1 cells and the proportion of Th1 cells within CD4 T cells from the LEAN group to the OB-NL group to the OB-NAFLD group, and both the number and proportion of Th1 cells were greater in the OB-NAFLD than in the OB-NL and LEAN groups (Figure 2*B*). Consistent with these findings, the proportion of CD4 T cells that produced interferon (IFN)-γ, the signature cytokine of Th1 cells, progressively increased from the LEAN group to the OB-NL group to the OB-NAFLD group, and was greater in the OB-NAFLD than the OB-NL and LEAN groups (Figure 2*C*, Supplementary Figure 3*C*). There were no differences in the total number of Th17 cells or the proportion of CD4 T cells that were Th17 cells among the 3 groups (Figure 2*B*). However, the proportion of CD4 T cells that produced interleukin (IL)17 was lower in the OB-NL and OB-NAFLD groups than in the LEAN group (Figure 2*C*, Supplementary Figure 5*B*). Within CD8 T cells, the proportion that produced IFN-γ progressively increased from the LEAN group to the OB-NL group to the OB-NAFLD group and was greater in the OB-NAFLD than the OB-NL and LEAN groups (Figure 2*C*). A very small percentage of stimulated CD8 T cells produced IL17 and the proportion that produced IL17 was lower in the OB-NAFLD than in the LEAN group (Figure 2*C*). The number of AT $CD69^+$ CD4 T cells, which are composed of recently activated and tissue-resident memory T cells, was greater in the OB-NAFLD group than in the OB-NL and LEAN groups (Figure 2*D*). The number of $CD69^+$ CD8 T cells and $CD69^+$ natural killer cells increased progressively from the LEAN group to the OB-NL group to the OB-NAFLD group and were significantly greater in the OB-NAFLD group than in the LEAN group, without a difference between the 2 obese groups (Figure 2*D*).

We then evaluated the relationship between insulin sensitivity and the subgroups of proinflammatory T cells that showed significantly greater numbers or percentages in the OB-NAFLD group than the OB-NL group (ie, % memory CD4 T cells, % memory CD8 T cells, total and % Th1 T cells, % IFN-γ^+ CD4 and CD8 T cells, and total $CD69^+$ CD4 T cells). There were statistically significant, but weak, inverse correlations between muscle insulin sensitivity and these T-cell subgroups (Supplementary Figure 6).

No significant differences were identified among the 3 groups of participants in the numbers of AT neutrophils, B cells, eosinophils, or mast cells (Supplementary Figure 4). There were also no differences among groups in the number or proportion of Th2 cells (Supplementary Figure 5*A*), the proportion of CD4 T cells that produced IL22 alone or in combination with IL17, or in the proportion of CD4 and CD8 T cells that produced TNF-α or IL10 (Supplementary Figure 5*B*).

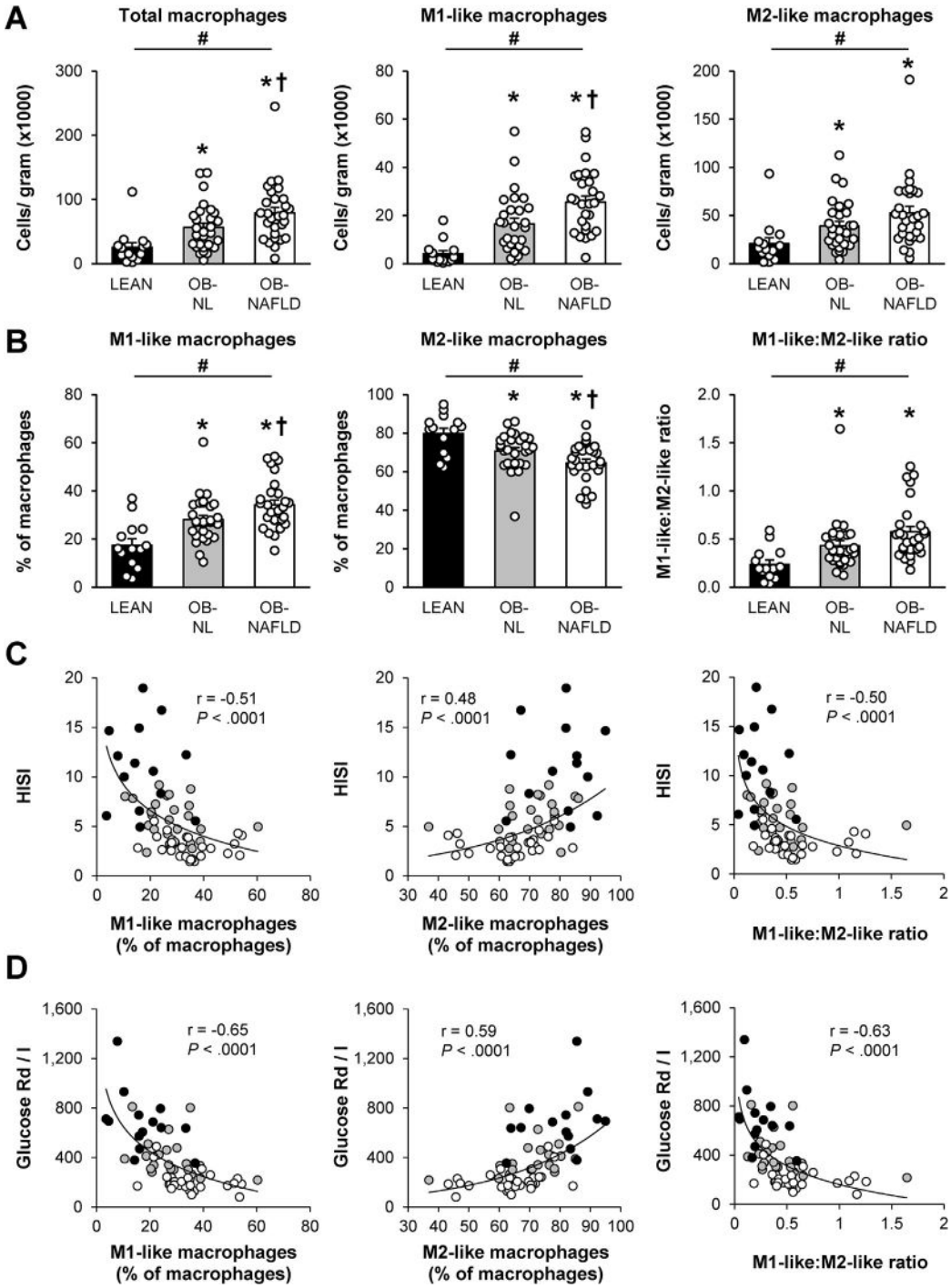

Figure 1. Macrophages in SAAT. (*A* and *B*) Number of total, pro-inflammatory (M1-like), and anti-inflammatory (M2-like) macrophages per gram of tissue (*A*) and M1-like and M2-like macrophages as a percentage of total macrophages and the M1-like:M2-like ratio (*B*) in SAAT in LEAN, OB-NL, and OB-NAFLD groups. (*C* and *D*) Relationship between the hepatic (Hepatic Insulin Sensitivity Index [HISI]; (*C*) and skeletal muscle (glucose rate of disappearance from plasma relative to plasma insulin concentration during the hyperinsulinemic-euglycemic clamp procedure [glucose Rd/I]; *D*) insulin sensitivity and M1-like and M2-like macrophages as a proportion of total macrophages and the M1-like:M2-like ratio in LEAN (*black circles*), OB-NL (*grey circles*), and OB-NAFLD (*white circles*) participants. The values in (*A*) and (*B*) are means ± SEM. *Value significantly different from the LEAN value, $P < .05$. †Value significantly different from the OB-NL value, $P < .05$. #Linear trend, $P < .05$.

AT Gene Expression of Markers of Inflammation are Increased in OB-NAFLD

AT expression of genes that encode for proinflammatory proteins, *SERPINE1*, *TNF*, *IL6*, *CCL2*, *CCL3*, *CCL5*, and *CXCL16*, macrophage (*CD68* and *MRC1*) and lipid-associated macrophage (*TREM2*) markers, and an anti-inflammatory protein (*IL10*) progressively increased from the LEAN group to the OB-NL group to the OB-NAFLD group, but there was no

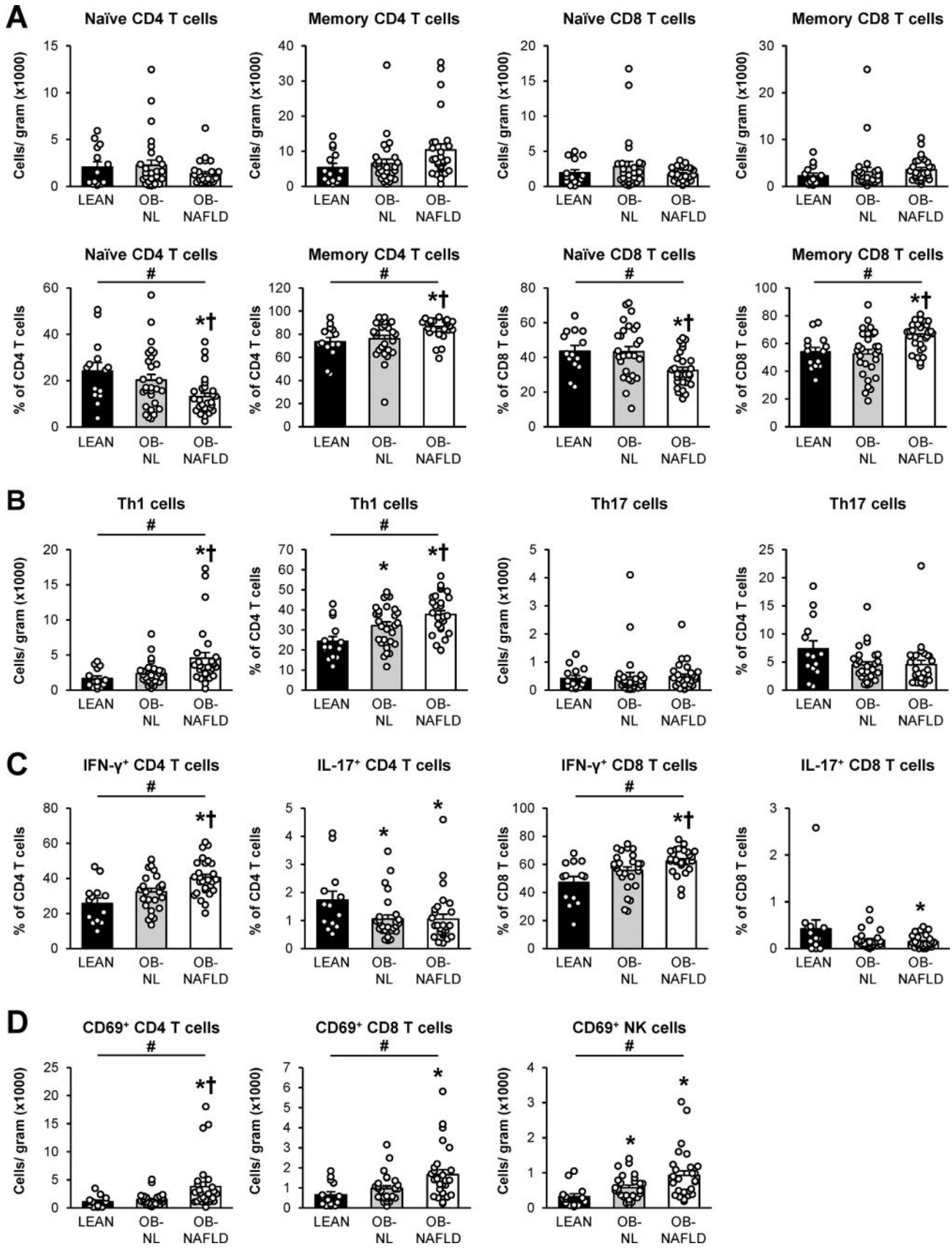

Figure 2. T cells in SAAT. (*A*) Absolute numbers (*top row*) and proportions (*bottom row*) of naïve and memory CD4 and CD8 T cells. (*B*) Absolute Th1 and Th17 cell numbers and proportions within total CD4 T cells. (*C*) Frequencies of IFN-γ- and IL17-positive cells within CD4 (*left 2 graphs*) and CD8 (*right 2 graphs*) T cells, following in vitro stimulation. (*D*) Absolute numbers of $CD69^+$ CD4, CD8, and natural killer (NK) cells. Values are means ± SEM. *Value significantly different from the LEAN value, $P < .05$. †Value significantly different from the OB-NL value, $P < .05$. #Linear trend, $P < .05$.

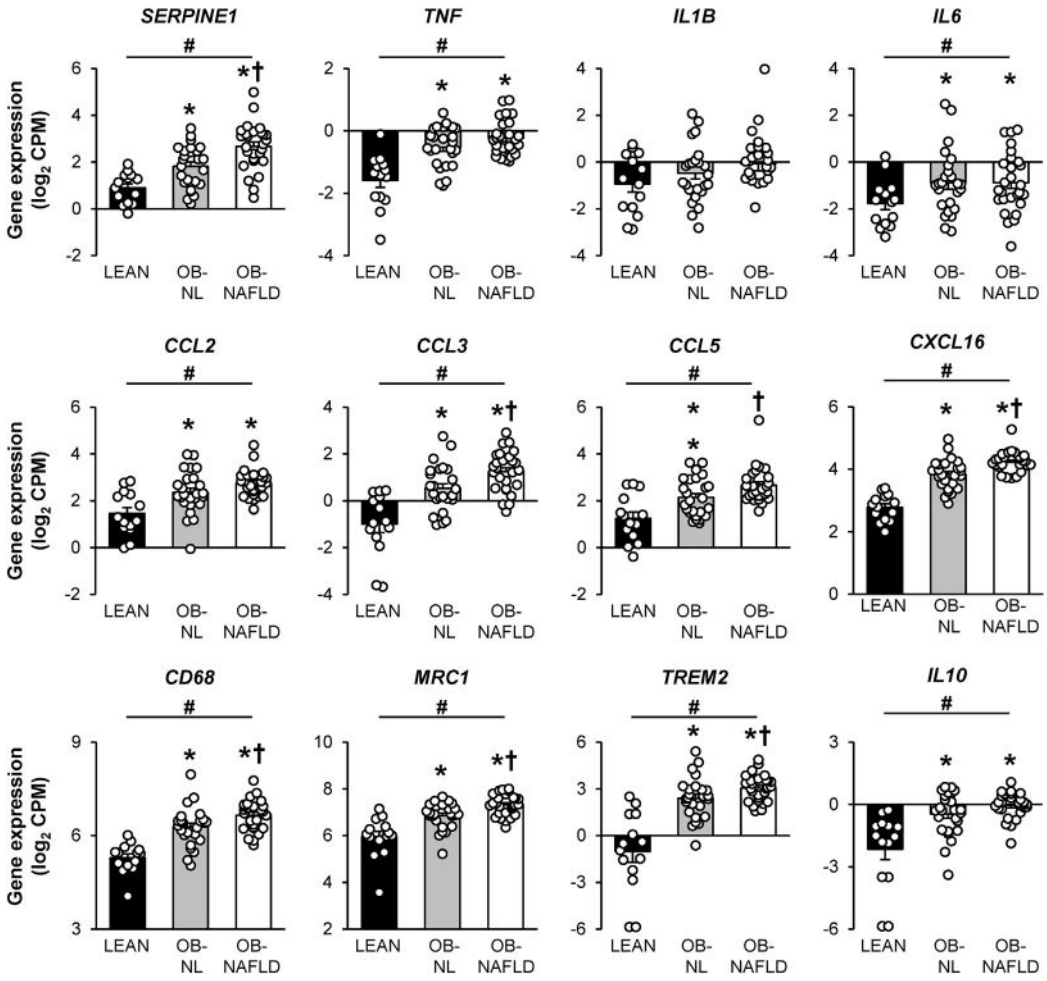

Figure 3. Gene expression of markers of inflammation in SAAT. Expression of genes encoding for cytokines (PAI-1 [encoded by *SERPINE1*], TNF-α, IL1β, IL6, CCL2, CCL3, CCL5, CXCL16, IL10) and for proteins highly expressed in macrophages (CD68 and CD206, encoded by *MRC1*) and lipid-associated macrophages (TREM2) in SAAT in LEAN, OB-NL, and OB-NAFLD groups. Values are means ± SEM *Value significantly different from the LEAN value, $P < .05$. †Value significantly different from the OB-NL value, $P < .05$. #Linear trend, $P < .05$.

difference in *IL1B* expression among the groups (Figure 3). Moreover, the expression of genes that encode for *SERPINE1*, *CCL3*, *CCL5*, *CXCL16*, *CD68*, *MRC1*, and *TREM2* were greater in the OB-NAFLD group than in the OB-NL group and greater in the OB-NL group than in the LEAN group (Figure 3). The expression of genes that encode for several other proinflammatory proteins (*TNF*, *IL6*, and *CCL2*) were greater in the OB-NL and OB-NAFLD groups than in the LEAN group, but not different between the 2 obese groups.

Concentrations of Plasma PAI-1 But Not Cytokines are Greater in the OB-NAFLD Group Than the OB-NL Group

To provide a more comprehensive assessment of circulating cytokines than would be obtained by fasting samples only, we evaluated plasma cytokine concentrations serially for 24 hours (every hour from 0700 hours to 2300 hours and then at 0500 hours and 0700 hours the next day). With the exception of the diurnal variation in plasma PAI-1 concentrations, plasma TNF-α, IL6, IFN-γ, CCL2, CCL5, IL1β, and IL17 concentrations were stable throughout the 24-hour blood sampling study and were not affected by meals (consumed at 0700 hours, 1300 hours, and 1900 hours) (Figure 4). The 24-hour plasma TNF-α and CCL2 concentration AUCs were greater in the OB-NL and OB-NAFLD groups than in the LEAN group, without differences between the 2 obese groups. The 24-hour plasma IL6, IFN-γ, CCL5, IL1β, and IL17 concentration AUCs were not significantly different between the groups. Plasma PAI-1 progressively increased from the LEAN group to the OB-NL group to the OB-NAFLD group and the 24-hour AUC was greater in the OB-NAFLD group than in both OB-NL and LEAN groups (Figure 4). Because of the unique differences in plasma PAI-1 concentration among the 3 groups of participants, which was not observed with the other plasma cytokines, we evaluated the relationship between 24-hour plasma PAI-1 AUC and insulin sensitivity among all participants. There was an inverse curvilinear correlation between 24-hour plasma PAI-1 AUC and both hepatic and skeletal muscle insulin sensitivity (Figure 5*A*). In addition, there was a positive correlation between markers of ATMs

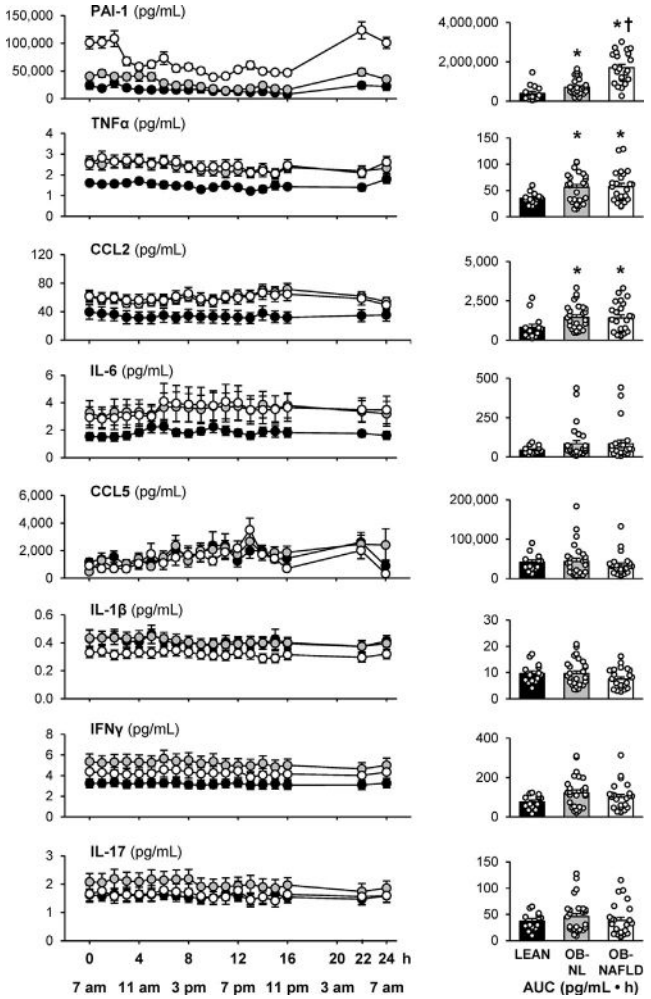

Figure 4. 24-h plasma cytokine profiles. Plasma cytokine concentrations determined hourly between 7 am and 11 pm on day 1 and at 5 am and 7 am on day 2 (*left panels*) and 24-h AUCs (*right panels*) in LEAN, OB-NL, and OB-NAFLD groups. Values are means ± SEM. *Value significantly different from the LEAN value, $P < .05$. †Value significantly different from the OB-NL value, $P < .05$.

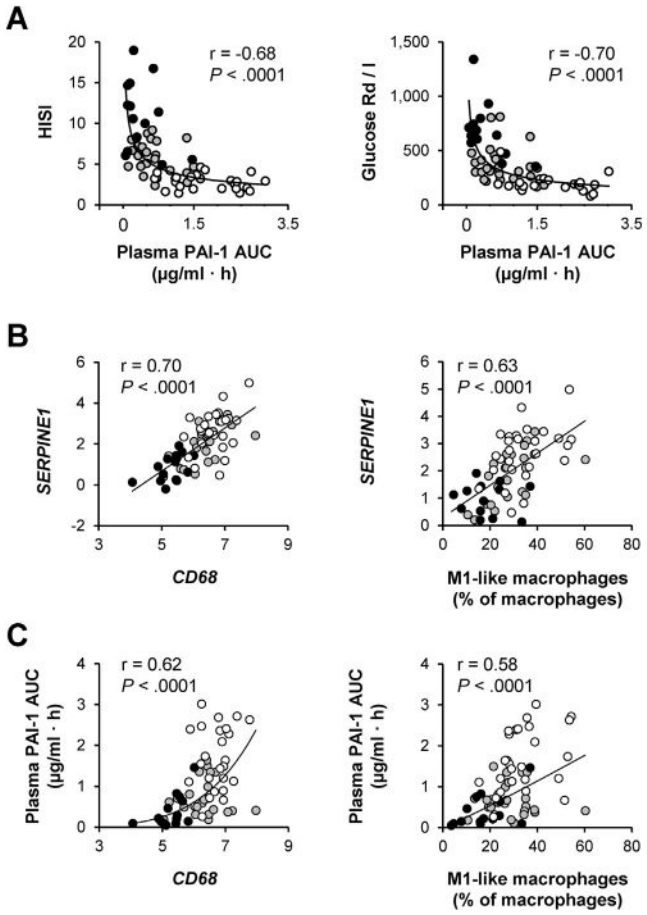

Figure 5. Relationships among plasma PAI-1 24-h AUC and both hepatic (Hepatic Insulin Sensitivity Index [HISI]) and skeletal muscle (glucose rate of disappearance from plasma relative to plasma insulin concentration during the hyperinsulinemic-euglycemic clamp procedure [glucose Rd/I]) insulin sensitivity (*A*), AT *SERPINE1* expression and both AT *CD68* expression and M1-like macrophages (*B*), and plasma PAI-1 24-h AUC and both AT *CD68* expression and M1-like macrophages (*C*) in LEAN (*black circles*), OB-NL (*grey circles*), and OB-NAFLD (*white circles*) participants.

(expression of *CD68* and percentage of M1-like ATMs) and both AT expression of *SERPINE1* and 24-hour plasma PAI-1 AUC (Figures 5*B* and 5*C*).

Plasma and AT Exosomes From OB-NAFLD Induce Insulin Resistance in Myotubes and Hepatocytes

Exosomes isolated from plasma and SAAT explant cultures were used to assess their effects on insulin action in myotubes and hepatocytes. The reliability of our isolation procedure was verified by measuring particle size (Supplementary Figure 7*A*) and the expression of exosome-specific protein markers (Supplementary Figures 7*B* and 7*C*). Plasma exosome concentration was 3-fold higher in the OB-NAFLD group than in the OB-NL and LEAN groups (7.0 ± 1.5 vs 2.5 ± 0.3 and 2.0 ± 0.3 10^{10} particles/mL, respectively; $P < .01$). We detected protein markers of AT-derived exosomes in plasma exosome samples (Supplementary Figure 7*D*), demonstrating that the plasma exosomes originated, at least in part, from AT. Compared with exosomes derived from the LEAN and OB-NL groups, plasma and SAAT–derived exosomes from the OB-NAFLD group caused insulin resistance in both myotubes and hepatocytes, demonstrated by impaired insulin signaling (phosphorylation of Akt; Figures 6*A* and 6*B*). Equal concentrations of exosomes were used to treat myotubes and hepatocytes ex vivo to evaluate the concentration-independent effects of exosomes on insulin action across study groups. Therefore, it is possible the adverse effects of plasma exosomes on insulin action in the OB-NAFLD group might be more pronounced in vivo because of their higher plasma exosome concentrations. The effects of both plasma and SAAT–derived exosomes on insulin signaling in myotubes and hepatocytes ex vivo correlated directly with skeletal muscle and hepatic insulin sensitivity, respectively, measured in vivo using the clamp procedure and stable isotopically labeled glucose tracer infusion (Figures 6*C* and 6*D*).

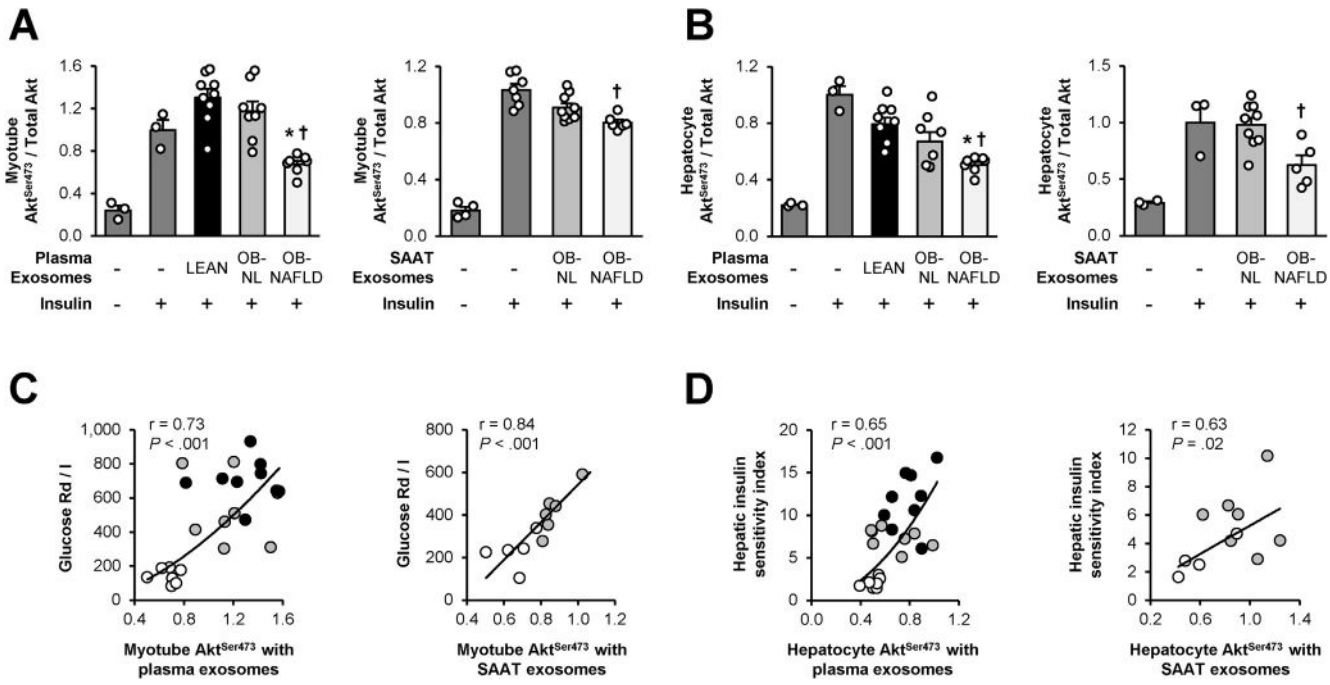

Figure 6. Exosomes and insulin action. (*A* and *B*) Insulin-stimulated phosphorylation of serine 473 of Akt in human skeletal muscle myotubes (*A*) and mouse hepatocytes (*B*) treated with exosomes isolated from plasma from LEAN, OB-NL, and OB-NAFLD participants and SAAT explants from OB-NL and OB-NAFLD participants. (*C*) Relationship between skeletal muscle insulin sensitivity (glucose rate of disappearance from plasma relative to plasma insulin concentration during the hyperinsulinemic-euglycemic clamp procedure [glucose Rd/I]) and phosphorylation of serine 473 of Akt in myotubes treated with exosomes isolated from plasma and SAAT in LEAN (*black circles*), OB-NL (*grey circles*), and OB-NAFLD (*white circles*) participants. (*D*) Relationship between the Hepatic Insulin Sensitivity Index (HISI) and phosphorylation of serine 473 of Akt in hepatocytes treated with exosomes isolated from plasma and SAAT in LEAN (*black circles*), OB-NL (*grey circles*), and OB-NAFLD (*white circles*) participants. Values are means ± SEM. *Value significantly different from the LEAN value, $P < .05$. †Value significantly different from the OB-NL value, $P < .05$.

Discussion

We conducted in vivo and ex vivo studies to assess the potential importance of SAAT inflammation and exosomes in the pathogenesis of insulin resistance in people with obesity and NAFLD. The immune cell profile and expression of genes involved in inflammation in SAAT, plasma cytokine concentrations, and the effect of both plasma and SAAT–derived exosomes on insulin action were evaluated in 3 rigorously characterized cohorts stratified by adiposity, metabolic health, and IHTG content. Our data demonstrate that most proinflammatory immune cells and the expression of proinflammatory genes in SAAT progressively increased from the LEAN group to the OB-NL group to the OB-NAFLD group. Moreover, these markers of inflammation were often significantly greater in the OB-NAFLD group than in the OB-NL group, including: (1) the number of total and proinflammatory (M1-like) macrophages and the percentage of macrophages that were M1-like; (2) the number or percentage of activated and memory T-cell subsets (memory CD4 and CD8 T cells, IFN-γ–producing CD4 and CD8 T cells, and $CD69^+$ CD4 T cells); and (3) gene expression of proinflammatory cytokines (*SERPINE 1*, *CCL3*, *CCL5*, and *CXCL16*) and macrophage markers (*CD68* and *MRC1*) and lipid-associated macrophage (*TREM2*) markers. However, the absolute mean differences in immune cells and gene expression between the OB-NL and the OB-NAFLD groups were small, and there was considerable overlap in individual participant values between the 2 obese groups. There were no differences in the 24-hour plasma cytokine AUCs between the OB-NL and OB-NAFLD groups with the exception of PAI-1, which was much greater in the OB-NAFLD group than in the OB-NL and LEAN groups and was inversely correlated with measures of both hepatic and skeletal muscle insulin sensitivity. Both plasma and SAAT exosomes isolated from the OB-NAFLD group impaired insulin action in myotubes and hepatocytes ex vivo. In addition, the percentage of macrophages that were proinflammatory, which are an important source of plasma and AT–derived exosomes, was inversely correlated with both hepatic and skeletal muscle insulin sensitivity. Together, these results demonstrate it is unlikely that SAAT inflammation causes systemic insulin resistance by increasing the release of classical inflammatory cytokines into the circulation. Instead, our data suggest SAAT production and secretion of PAI-1 and exosomes are involved in the pathogenesis of insulin resistance associated with obesity and NAFLD, but we are unable to precisely determine whether these relationships are causal or simply an association.

We found a greater number of total ATMs and M1-like ATMs per gram of SAAT in the OB-NAFLD group than the OB-NL group, although the 2 groups were matched on body fat mass. Therefore, other factors, independent of fat mass

itself, are involved in the accumulation of SAAT ATMs in people with obesity and NAFLD. The factors responsible for the infiltration and polarization of immune cells in AT have been studied in rodent models. Macrophage infiltration increases in response to hypoxia[29] and increased rates of lipolysis of adipocyte TGs.[30] Moreover, increased intra-adipocyte free fatty acid flux can cause adipocyte hypoxia by adenine nucleotide translocase-2–dependent uncoupling of mitochondrial respiration.[31] In addition, increases in CD8 T cells and CD4 Th1 cells in obese rodents increase the secretion of chemokines that recruit circulating monocytes to AT and promote their differentiation into macrophages,[12,32] which are then polarized toward a proinflammatory state using IFN-γ.[33] The release of cytokines from M1-like macrophages also increases macrophage number in a positive, feed-forward manner by increasing monocyte infiltration and stimulating the proliferation of tissue-resident macrophages.[34–36] Together, these data suggest a complex interplay among AT free fatty acid flux, oxygenation, and immune cells that drive the recruitment and accumulation of proinflammatory ATMs.

Both hepatic and skeletal muscle insulin sensitivity were lower in the OB-NAFLD group than the OB-NL group. Although the number and percentage of M1-like macrophages and many proinflammatory T-cell subsets and SAAT expression of proinflammatory genes were greater in the OB-NAFLD group than the OB-NL group, these differences did not translate into differences in classical plasma cytokine concentrations. Instead, SAAT gene expression of *SERPINE1*, which encodes for PAI-1, progressively increased from the LEAN group to the OB-NL group to the OB-NAFLD groups, and plasma PAI-1 24-hour AUC was inversely associated with hepatic and muscle insulin sensitivity. These findings are consistent with the results from previous studies that found plasma PAI-1 concentrations are increased in people with NAFLD.[37] PAI-1 is produced by adipocytes[38,39] and ATMs.[38,40] The correlations we observed between ATMs and both AT expression of *SERPINE1* and 24-hour plasma PAI-1 AUC support the notion that the increase in plasma PAI-1 concentrations in the OB-NAFLD group was, at least in part, caused by the production of PAI-1 by ATMs. In rodent models, adipocyte-specific PAI-1 overexpression causes insulin resistance[41] whereas whole-body and adipocyte-specific knockouts of PAI-1 improve insulin action.[42,43] These findings suggest the production of most cytokines by SAAT might have local paracrine effects, but do not have direct effects on systemic metabolic function. In fact, it is unlikely that changes in circulating TNF-α, IL1β, and IL6 cause systemic insulin resistance in people because: (1) biological treatments that decrease TNF-α and IL1β plasma concentrations or activity do not affect insulin sensitivity[44–47]; (2) TNF-α concentrations that impair glucose uptake or insulin signaling in cell systems are orders of magnitude higher than plasma concentrations found in people[48,49]; (3) the infusion of IL6 that results in a 25- to 160-fold increase in plasma IL6 concentrations in healthy lean people has either no effect[50,51] or a small beneficial effect on insulin sensitivity[52]; and (4) TNF-α infusions that cause about a 10-fold increase in plasma concentrations (from 1–2 pg/mL to ~16 pg/mL) reduce insulin-stimulated glucose uptake by only 10%–15%.[51,53] Together, these data suggest PAI-1 secreted from AT, but not other adipokines, contributed to hepatic and muscle insulin resistance observed in our OB-NAFLD participants.

The marked increase in plasma exosomes observed in our OB-NAFLD group than in the OB-NL and LEAN groups extends the findings from previous studies that demonstrated plasma exosome concentrations were higher in people with obesity and metabolic syndrome[54] and in people with obesity and type 2 diabetes[55] than in healthy lean subjects. Incubating human skeletal muscle myotubes and mouse hepatocytes with plasma and SAAT–derived exosomes obtained from the OB-NAFLD group, but not from the LEAN or OB-NL groups, impaired insulin-stimulated Akt phosphorylation. Moreover, the effects of both plasma and SAAT–derived exosomes on insulin signaling in myotubes and hepatocytes correlated directly with skeletal muscle and hepatic insulin sensitivity, respectively, measured in vivo during the clamp procedure. In mouse models, injecting ATM exosomes isolated from lean mice into obese mice improves systemic insulin sensitivity, whereas injecting exosomes isolated from ATMs from obese mice induces insulin resistance in lean mice.[21,22] It is likely that exosome-mediated regulation of insulin action is mediated by the transfer of specific miRNAs; studies conducted in mice and cell culture systems have shown exosomal miR-29a and miR-155 decrease[21,22] and exosomal miR-690 increase[56] insulin sensitivity. Our results support the notion that circulating exosomes derived from SAAT contribute to systemic insulin resistance in people with obesity and NAFLD, but does not preclude the possibility that exosomes produced by other organs are also involved.

The results from the present study demonstrate statistically significant, but small, differences in SAAT immune cell populations and SAAT expression of most proinflammatory cytokines in people with obesity and NAFLD than in those with obesity and normal IHTG content. Although it has been proposed that the secretion of proinflammatory cytokines cause systemic insulin resistance, this seems unlikely because 24-hour plasma concentrations of many classical cytokines were not greater in the OB-NAFLD group than the OB-NL group. Instead, our data, in conjunction with the results from previous studies conducted in mouse models, suggest SAAT-derived PAI-1 and exosomes are involved in the pathogenesis of insulin resistance in people with obesity and NAFLD.

Supplementary Material

Note: To access the supplementary material accompanying this article, visit the online version of *Clinical Gastroenterology and Hepatology* at www.cghjournal.org, and at https://doi.org/10.1053/j.gastro.2021.05.008.

References

1. Klein S, Wadden T, Sugerman HJ. AGA technical review on obesity. Gastroenterology 2002;123:882–932.

2. Fabbrini E, Magkos F, Mohammed BS, et al. Intrahepatic fat, not visceral fat, is linked with metabolic complications of obesity. Proc Natl Acad Sci U S A 2009; 106:15430–15435.
3. Stefan N, Haring HU, Cusi K. Non-alcoholic fatty liver disease: causes, diagnosis, cardiometabolic consequences, and treatment strategies. Lancet Diabetes Endocrinol 2019;7:313–324.
4. Stender S, Kozlitina J, Nordestgaard BG, et al. Adiposity amplifies the genetic risk of fatty liver disease conferred by multiple loci. Nat Genet 2017;49:842–847.
5. Belfort R, Harrison SA, Brown K, et al. A placebo-controlled trial of pioglitazone in subjects with nonalcoholic steatohepatitis. N Engl J Med 2006;355: 2297–2307.
6. Sanyal AJ, Chalasani N, Kowdley KV, et al. Pioglitazone, vitamin E, or placebo for nonalcoholic steatohepatitis. N Engl J Med 2010;362:1675–1685.
7. Kawai T, Autieri MV, Scalia R. Adipose tissue inflammation and metabolic dysfunction in obesity. Am J Physiol Cell Physiol 2021;320:C375–C391.
8. Russo L, Lumeng CN. Properties and functions of adipose tissue macrophages in obesity. Immunology 2018; 155:407–417.
9. Hotamisligil GS, Shargill NS, Spiegelman BM. Adipose expression of tumor necrosis factor-alpha: direct role in obesity-linked insulin resistance. Science 1993;259: 87–91.
10. Uysal KT, Wiesbrock SM, Marino MW, et al. Protection from obesity-induced insulin resistance in mice lacking TNF-alpha function. Nature 1997;389:610–614.
11. Feuerer M, Herrero L, Cipolletta D, et al. Lean, but not obese, fat is enriched for a unique population of regulatory T cells that affect metabolic parameters. Nat Med 2009;15:930–939.
12. **Winer S, Chan Y**, Paltser G, et al. Normalization of obesity-associated insulin resistance through immunotherapy. Nat Med 2009;15:921–929.
13. Wentworth JM, Naselli G, Brown WA, et al. Pro-inflammatory CD11c+CD206+ adipose tissue macrophages are associated with insulin resistance in human obesity. Diabetes 2010;59:1648–1656.
14. **Fabbrini E, Cella M**, McCartney SA, et al. Association between specific adipose tissue CD4+ T-cell populations and insulin resistance in obese individuals. Gastroenterology 2013;145:366–374.
15. Klimcakova E, Roussel B, Kovacova Z, et al. Macrophage gene expression is related to obesity and the metabolic syndrome in human subcutaneous fat as well as in visceral fat. Diabetologia 2011;54:876–887.
16. **Amouzou C, Breuker C, Fabre O**, et al. Skeletal muscle insulin resistance and absence of inflammation characterize insulin-resistant Grade I obese women. PLoS One 2016;11:e0154119.
17. Kloting N, Fasshauer M, Dietrich A, et al. Insulin-sensitive obesity. Am J Physiol Endocrinol Metab 2010;299:E506–E515.
18. Verboven K, Wouters K, Gaens K, et al. Abdominal subcutaneous and visceral adipocyte size, lipolysis and inflammation relate to insulin resistance in male obese humans. Sci Rep 2018;8:4677.
19. Crewe C, Scherer PE. Intercellular and interorgan crosstalk through adipocyte extracellular vesicles. Rev Endocr Metab Disord 2021. https://doi.org/10.1007/s11154–020-09625-x. In press.
20. Deng ZB, Poliakov A, Hardy RW, et al. Adipose tissue exosome-like vesicles mediate activation of macrophage-induced insulin resistance. Diabetes 2009; 58:2498–2505.
21. Ying W, Riopel M, Bandyopadhyay G, et al. Adipose tissue macrophage-derived exosomal miRNAs can modulate in vivo and in vitro insulin sensitivity. Cell 2017; 171:372–384.e12.
22. Liu T, Sun YC, Cheng P, et al. Adipose tissue macrophage-derived exosomal miR-29a regulates obesity-associated insulin resistance. Biochem Biophys Res Commun 2019;515:352–358.
23. Thomou T, Mori MA, Dreyfuss JM, et al. Adipose-derived circulating miRNAs regulate gene expression in other tissues. Nature 2017;542:450–455.
24. **Cifarelli V, Beeman SC**, Smith GI, et al. Decreased adipose tissue oxygenation associates with insulin resistance in individuals with obesity. J Clin Invest 2020; 130:6688–6699.
25. Allison DB, Paultre F, Maggio C, et al. The use of areas under curves in diabetes research. Diabetes Care 1995; 18:245–250.
26. Ghosh D, Vogt A. Outliers: an evaluation of methodologies. Joint Statistical Meetings Proceedings: American Statistical Association 2012:3455–3460.
27. Lesna IK, Cejkova S, Kralova A, et al. Human adipose tissue accumulation is associated with pro-inflammatory changes in subcutaneous rather than visceral adipose tissue. Nutr Diabetes 2017;7:e264.
28. **Hill DA, Lim HW**, Kim YH, et al. Distinct macrophage populations direct inflammatory versus physiological changes in adipose tissue. Proc Natl Acad Sci U S A 2018;115:E5096–E5105.
29. **Lee YS, Kim JW**, Osborne O, et al. Increased adipocyte O2 consumption triggers HIF-1alpha, causing inflammation and insulin resistance in obesity. Cell 2014; 157:1339–1352.
30. Kosteli A, Sugaru E, Haemmerle G, et al. Weight loss and lipolysis promote a dynamic immune response in murine adipose tissue. J Clin Invest 2010;120:3466–3479.
31. Seo JB, Riopel M, Cabrales P, et al. Knockdown of ANT2 reduces adipocyte hypoxia and improves insulin resistance in obesity. Nature Metabolism 2019;1:86–97.
32. Nishimura S, Manabe I, Nagasaki M, et al. CD8+ effector T cells contribute to macrophage recruitment and adipose tissue inflammation in obesity. Nat Med 2009; 15:914–920.
33. Mantovani A, Sica A, Sozzani S, et al. The chemokine system in diverse forms of macrophage activation and polarization. Trends Immunol 2004;25:677–686.
34. Oh DY, Morinaga H, Talukdar S, et al. Increased macrophage migration into adipose tissue in obese mice. Diabetes 2012;61:346–354.

35. Amano SU, Cohen JL, Vangala P, et al. Local proliferation of macrophages contributes to obesity-associated adipose tissue inflammation. Cell Metab 2014;19:162–171.
36. Kanda H, Tateya S, Tamori Y, et al. MCP-1 contributes to macrophage infiltration into adipose tissue, insulin resistance, and hepatic steatosis in obesity. J Clin Invest 2006;116:1494–1505.
37. Targher G, Chonchol M, Miele L, et al. Nonalcoholic fatty liver disease as a contributor to hypercoagulation and thrombophilia in the metabolic syndrome. Semin Thromb Hemost 2009;35:277–287.
38. Alessi MC, Peiretti F, Morange P, et al. Production of plasminogen activator inhibitor 1 by human adipose tissue: possible link between visceral fat accumulation and vascular disease. Diabetes 1997;46:860–867.
39. Eriksson P, Reynisdottir S, Lonnqvist F, et al. Adipose tissue secretion of plasminogen activator inhibitor-1 in non-obese and obese individuals. Diabetologia 1998; 41:65–71.
40. Kishore P, Li W, Tonelli J, et al. Adipocyte-derived factors potentiate nutrient-induced production of plasminogen activator inhibitor-1 by macrophages. Sci Transl Med 2010;2:20ra15.
41. Lijnen HR, Alessi MC, Van Hoef B, et al. On the role of plasminogen activator inhibitor-1 in adipose tissue development and insulin resistance in mice. J Thromb Haemost 2005;3:1174–1179.
42. Ma LJ, Mao SL, Taylor KL, et al. Prevention of obesity and insulin resistance in mice lacking plasminogen activator inhibitor 1. Diabetes 2004;53:336–346.
43. **Liang X, Kanjanabuch T**, Mao SL, et al. Plasminogen activator inhibitor-1 modulates adipocyte differentiation. Am J Physiol Endocrinol Metab 2006;290:E103–E113.
44. Ofei F, Hurel S, Newkirk J, et al. Effects of an engineered human anti-TNF-alpha antibody (CDP571) on insulin sensitivity and glycemic control in patients with NIDDM. Diabetes 1996;45:881–885.
45. Paquot N, Castillo MJ, Lefebvre PJ, et al. No increased insulin sensitivity after a single intravenous administration of a recombinant human tumor necrosis factor receptor: Fc fusion protein in obese insulin-resistant patients. J Clin Endocrinol Metab 2000;85:1316–1319.
46. Bernstein LE, Berry J, Kim S, et al. Effects of etanercept in patients with the metabolic syndrome. Arch Intern Med 2006;166:902–908.
47. Everett BM, Donath MY, Pradhan AD, et al. Anti-inflammatory therapy with Canakinumab for the prevention and management of diabetes. J Am Coll Cardiol 2018; 71:2392–2401.
48. Hotamisligil GS, Murray DL, Choy LN, et al. Tumor necrosis factor alpha inhibits signaling from the insulin receptor. Proc Natl Acad Sci U S A 1994;91:4854–4858.
49. del Aguila LF, Claffey KP, Kirwan JP. TNF-alpha impairs insulin signaling and insulin stimulation of glucose uptake in C2C12 muscle cells. Am J Physiol 1999; 276:E849–E855.
50. Steensberg A, Fischer CP, Sacchetti M, et al. Acute interleukin-6 administration does not impair muscle glucose uptake or whole-body glucose disposal in healthy humans. J Physiol 2003;548:631–638.
51. Krogh-Madsen R, Plomgaard P, Moller K, et al. Influence of TNF-alpha and IL-6 infusions on insulin sensitivity and expression of IL-18 in humans. Am J Physiol Endocrinol Metab 2006;291:E108–E114.
52. **Carey AL, Steinberg GR**, Macaulay SL, et al. Interleukin-6 increases insulin-stimulated glucose disposal in humans and glucose uptake and fatty acid oxidation in vitro via AMP-activated protein kinase. Diabetes 2006; 55:2688–2697.
53. **Plomgaard P, Bouzakri K**, Krogh-Madsen R, et al. Tumor necrosis factor-alpha induces skeletal muscle insulin resistance in healthy human subjects via inhibition of Akt substrate 160 phosphorylation. Diabetes 2005; 54:2939–2945.
54. Eguchi A, Lazic M, Armando AM, et al. Circulating adipocyte-derived extracellular vesicles are novel markers of metabolic stress. J Mol Med (Berl) 2016; 94:1241–1253.
55. **Freeman DW, Noren Hooten N**, Eitan E, et al. Altered extracellular vesicle concentration, cargo, and function in diabetes. Diabetes 2018;67:2377–2388.
56. **Ying W, Gao H**, Dos Reis FCG, et al. MiR-690, an exosomal-derived miRNA from M2-polarized macrophages, improves insulin sensitivity in obese mice. Cell Metab 2021;33:781–790.

Author names in bold designate shared co-first authorship.

Received February 22, 2021. Accepted May 6, 2021.

Correspondence
Address correspondence to: Samuel Klein, MD, Center for Human Nutrition, Washington University School of Medicine, 660 S. Euclid Avenue, Campus Box 8031, St. Louis, Missouri 63110. e-mail: sklein@wustl.edu.

Acknowledgments
The authors thank the staff of the Center for Human Nutrition, the Clinical and Translational Research Unit, and the Center for Clinical Imaging Research for their help in performing this study, and the study subjects for their participation. Technical support for the mass cytometry analysis was provided by Washington University's Immunomonitoring Laboratory, which is supported by the Andrew M. and Jane M. Bursky Center for Human Immunology and Immunotherapy Programs.

Anja Fuchs, Dmitri Samovski, and Gordon I. Smith contributed equally.

CRediT Authorship Contributions

Anja Fuchs, PhD (Data curation: Equal; Formal analysis: Equal; Methodology: Equal; Writing – original draft: Equal).

Dmitri Samovski, PhD (Data curation: Equal; Formal analysis: Equal; Methodology: Equal; Writing – original draft: Equal).

Gordon I. Smith, PhD (Data curation: Equal; Formal analysis: Equal; Project; administration: Equal; Writing – original draft: Equal).

Vincenza Cifarelli, PhD (Data curation: Supporting; Writing – review & editing: Equal).

Sarah S. Farabi, RN, PhD (Data curation: Equal; Writing – review & editing: Supporting).

Jun Yoshino, jyoshino@wustl.edu (Data curation: Equal; Formal analysis: Equal; Methodology: Equal; Writing – review & editing: Equal).

Terri Pietka, BA, MA (Data curation: Equal; Writing – review & editing: Supporting).

Shin-Wen Chang, BS (Data curation: Equal; Writing – review & editing: Supporting).

Sarbani Ghosh, MS (Data curation: Equal; Writing – review & editing: Supporting).

Terence M. Myckatyn, MD (Methodology: Lead; Writing – review & editing: Equal).

Samuel Klein, MD (Conceptualization: Lead; Formal analysis: Equal; Funding acquisition: Lead; Methodology: Equal; Project administration: Lead; Resources: Lead; Supervision: Lead; Writing – original draft: Equal).

Transcript Profiling

The RNA sequencing data have been deposited in the Gene Expression Omnibus (GEO) database, https://www.ncbi.nlm.nih.gov/geo (accession no. GSE156906).

Conflict of interest

S.K. receives research funding from Janssen Pharmaceuticals and serves on a Scientific Advisory Board for Merck Sharp and Dohme Corp. T.M.M. serves on the Advisory Board for Allergan Medical and RTI and received royalties for product development from RTI. The other authors disclose no conflicts.

Funding

This study was supported by National Institutes of Health grants P30DK56341 (Nutrition Obesity Research Center), DK20579 (Diabetes Research Center), DK052574 (Digestive Disease Research Center), and UL1TR002345 (Clinical and Translational Science Award) and support from the Longer Life Foundation, the Foundation for Barnes-Jewish Hospital, and the Centene Corporation contract (P19-00559) for the Washington University-Centene ARCH Personalized Medicine Initiative.

Supplementary Methods

Metabolic Testing

Serial plasma cytokine concentrations for 24-hour and hyperinsulinemic-euglycemic clamp procedure. Subjects were admitted to the Clinical Translational Research Unit at 1700 hours on day 1 for ~48 hours and consumed a standard meal (50% carbohydrate, 35% fat, 15% protein) containing one third of their estimated energy requirements[1] between 1800 hours and 1900 hours. At 0630 hours the next morning on day 2, a catheter was inserted into an antecubital vein for 24-hour serial blood sampling. Blood samples were obtained every hour from 0700 hours to 2300 hours on day 2 and at 0500 hours and 0700 hours on day 3. Meals were provided at 0700 hours, 1300 hours, and 1900 hours. Each meal contained one third of the participant's energy requirements and were comprised of 50% carbohydrate, 35% fat, and 15% protein. A hyperinsulinemic-euglycemic clamp procedure, in conjunction with stable isotopically labeled glucose tracer infusion, was conducted on day 3 to assess hepatic and skeletal muscle insulin sensitivity. At 0700 hours, a primed (8.0 μmol/kg) continuous (0.08 μmol/kg/min) infusion of [U-^{13}C]glucose (Cambridge Isotope Laboratories Inc., Andover, MA) was started through the existing intravenous catheter. An additional catheter was inserted into a radial artery to obtain arterial blood samples. After the infusion of glucose tracer for 210 minutes (basal period), insulin was infused for 210 minutes at a rate of 50 mU/m^2/min (initiated with a 2-step priming dose of 200 mU/m^2 body surface area/min for 5 minutes followed by 100 mU/m^2/min for 5 minutes). The infusion of [U-^{13}C]glucose was stopped during insulin infusion because of the expected decrease in hepatic glucose production.[2] Euglycemia (~100 mg/dL) was maintained using variable infusion of 20% dextrose enriched to ~1% with [U-^{13}C]glucose. Blood samples were obtained before beginning the tracer infusion and every 6–7 minutes during the final 20 minutes (total of 4 blood samples) of the basal and insulin infusion periods.

AT biopsies. SAAT was obtained from the periumbilical area during the basal period of the clamp procedure. After anesthetizing the skin by injection of 1% lidocaine, a small skin incision (~0.5 cm) was made and ~0.5 g of adipose tissue was aspirated through a 4-mm liposuction cannula (Tulip Medical Products, San Diego, CA) connected to a 60-mL syringe. Samples were immediately rinsed in ice-cold saline and frozen in liquid nitrogen before being stored at -80°C until processed for RNA sequencing. In addition, ~3 g of subcutaneous AT was obtained using aspiration, immediately placed in ice-cold saline, and then stored on ice for stromal vascular fraction (SVF) or exosome isolation on the same day.

Sample Analysis and Calculations

Glucose kinetics. Plasma glucose tracer-to-tracee ratios were determined using gas-chromatography/mass-spectrometry as previously described.[3] The Hepatic Insulin Sensitivity Index (HISI) was calculated as the inverse of the product of plasma insulin concentration and the endogenous glucose rate of appearance into the systemic circulation, determined by dividing the glucose tracer infusion rate by the average plasma glucose tracer-to-tracee ratio during the last 20 minutes of the basal and insulin infusion periods of the hyperinsulinemic-euglycemic clamp procedure.[4] Total glucose rate of disappearance (Rd) during insulin infusion was assumed to be equal to the sum of endogenous glucose rate of appearance into the bloodstream and the rate of infused glucose during the last 20 minutes of the clamp procedure. Skeletal muscle insulin sensitivity was calculated as glucose Rd expressed per kg fat-free mass divided by the average plasma insulin concentration (glucose Rd/I) during the final 20 minutes of the clamp procedure.[4]

Adipose tissue RNA sequencing. Total RNA was isolated from frozen SAAT samples by using QIAzol lysis reagent and a RNeasy mini kit (Qiagen, Valencia, CA) in combination with a RNase-free DNase Set (Qiagen) as we previously described.[5] Three SAAT samples from the OB-NL group and 1 from the OB-NAFLD group were excluded from further analysis due to poor RNA quality attributable to RNA degradation. Library preparation on the remaining samples was performed with total RNA and complementary DNA fragments sequenced on an Illumina NovaSeq 6000 (Illumina, San Diego, CA). Expression of individual genes are presented as log2-transformed counts per million reads.

AT SVF isolation. To isolate the SVF from AT, the sample was rinsed twice with phosphate-buffered saline (PBS) to remove blood introduced during the liposuction procedure before being transferred to gentleMACS C tubes (Miltenyi Biotec, Auburn, CA) containing digestion medium (RPMI 1640 with 2% fetal calf serum, penicillin-streptomycin, GlutaMAX, sodium pyruvate, and nonessential amino acids). Collagenase D (Roche, Indianapolis, IN) was then added to a final concentration of 2 mg/mL and the tissue was incubated by placing the tube for 20 minutes at 37°C with shaking at 150 rpm. The tissue was then transferred to a gentleMACS dissociator (Miltenyi Biotec) to dissociate any remaining tissue pieces. The resulting cell suspension was filtered through a 100-μm cell strainer, washed with digestion medium, and subjected to red blood cell lysis (RBC lysis buffer, Biolegend, San Diego, CA). Cell suspensions were then resuspended in culture medium (RPMI 1640 with 10% fetal calf serum, penicillin-streptomycin, GlutaMAX, sodium pyruvate, and nonessential amino acids) and stored on ice until further processing for mass cytometry or in vitro stimulation and flow cytometry.

Mass cytometry. For mass cytometry analysis, the SVF was isolated and the cells were subjected to Ficoll density centrifugation (GE Healthcare, Boston, MA; 400*g* for 20 minutes without break) to remove debris and RBCs. The interphase was collected and resuspended in PBS with 2% bovine calf serum and 0.05% sodium azide (Fluorescence-Activated Cell Sorting [FACS] buffer). Cells were incubated for 10 minutes on ice with Fc receptor block buffer prepared with 10% human plasma before incubation with metal isotype-conjugated antibodies for 60 minutes on ice. Antibodies used for mass cytometry are listed in Supplementary Table 3. After antibody incubation, cells were stained with 2.5 μmol/L cisplatin (Enzo Life Sciences, Farmingdale, NY) to detect dead cells, followed by fixation in 4%

paraformaldehyde (Electron Microscopy Sciences, Hatfield, PA). Stained and fixed samples were frozen in fetal calf serum with 10% dimethylsulfoxide at -80°C before mass cytometric analysis. On each day of SVF processing, a frozen aliquot of peripheral blood mononuclear cells (PBMCs) prepared from a healthy volunteer was thawed and then stained, fixed, and frozen in the same manner as the SVF samples. These PBMC samples served as reference samples to monitor day-to-day variations in staining intensity.

The day before mass cytometric acquisition, cells from all samples (SVF from 2 LEAN and 2 OB-NAFLD participants, and 4 PBMC reference samples) were thawed, washed, and then barcoded using Maxpar Pd barcoding reagents, according to the manufacturer's recommendations (Fluidigm, South San Francisco, CA). After barcoding, equal numbers from each barcoded sample were combined into 1 pooled sample and incubated with Cell-ID Intercalator-Ir (Fluidigm) to detect non-nucleated cells/debris and doublets, diluted in 2% paraformaldehyde, overnight. Cells were acquired on a CyTOF2/Helios instrument (Fluidigm) by Washington University's Immunomonitoring Laboratory. Samples were debarcoded using the program Single Cell Debarcoder.[6] Samples were analyzed with the FlowJo v10 software. Comparison of marker expression (CD45, CD14, HLA-DR, CD86) on monocytes within the PBMC reference samples revealed no more than 15% variance in signal intensity between processing days. Macrophages were gated as DNA^+ $cisplatin^-$, $CD45^+$ $CD64^+$ cells and then further divided into 3 main subsets based on their expression of CD206 and CD11c as specified in Supplementary Figure 2*A*. Each subset was further analyzed for expression levels (geometric mean) of each macrophage-expressed surface marker. A heat map was generated by setting the highest expression (detected in any of the 4 samples, within any of the 3 $CD64^+$ subsets) as 100% and calculating marker expression of the other samples and subsets as a percentage of this maximum value (Supplementary Figure 2 *B*)

In vitro stimulation. For intracellular cytokine staining, a portion of the cell suspensions from the SVF was cultured in wells of a 96-well round bottom plate at 37°C for 5 hours in the presence of GolgiPlug (Brefeldin A, BD Biosciences, San Jose, CA) and 50 ng/mL phorbol 12-myristate 13-acetate (PMA) and 1 μg/mL ionomycin (both from Sigma Aldrich, St. Louis, MO). After the culture period, cells were processed for flow cytometric staining as indicated in the next section.

Flow cytometry. Before antibody staining, cells isolated from AT were incubated on ice with Fc receptor block buffer consisting of FACS buffer mixed with 10% autologous plasma. Cells were then incubated with fluorochrome-conjugated antibody cocktails, diluted in Fc receptor block buffer, for 20 minutes on ice. Details of the antibody cocktails used in this study are shown in Supplementary Table 4. After antibody staining, cells were washed with PBS and incubated with Zombie Aqua fixable live/dead dye (Biolegend) diluted in PBS. Subsequently, cells were fixed in Cytofix buffer (BD Biosciences), washed with FACS buffer, and stored at 4°C prior to flow cytometric analysis. Cell concentrations in stained samples were determined by adding counting beads to the lymphocyte-stained cell sample immediately before flow cytometric acquisition (123count eBeads, eBioscience, San Diego, CA). Cell concentrations in samples were calculated per the manufacturer's directions and were used to estimate the cell counts per gram of adipose tissue. For intracellular cytokine staining, surface-stained, fixed cells were washed with permeabilization buffer (PBS with 0.5% saponin and 0.1% bovine serum albumin), followed by incubation with anti-cytokine antibodies as specified in Supplementary Table 4, diluted in permeabilization buffer for 30 minutes at room temperature. Cells were then washed with permeabilization buffer and resuspended in FACS buffer. Samples were acquired on an LSR Fortessa using Diva software and analyzed with the FlowJo v10 software (all from BD Biosciences, San Jose, CA). Cells were gated on single, live, $CD45^+$ cells. Analysis of the individual immune cell subsets was performed as specified in Supplementary Figure 8 and Supplementary Table 5.

AT explant culture. SAAT was minced into small (~2 mm) pieces, repeatedly washed with PBS, and processed to eliminate any visible connective tissue and blood vessels. The minced tissue was centrifuged (300*g*, 5 minutes) to remove RBCs and debris, and incubated in serum-free M199 medium supplemented with 0.1% (vol/vol) of bovine serum albumin and 1% (vol/vol) of penicillin-streptomycin solution (all from Sigma-Aldrich) at 37°C in an atmosphere containing 5% CO_2 (1 g of tissue/3 mL of media). The medium was renewed after 2 hours and the explants were cultured for an additional 48 hours. The conditioned media were collected, centrifuged (300*g*, 5 minutes), and stored at -80°C until further analysis.

Plasma and AT exosome isolation. Plasma and AT–derived exosomes were isolated as previously described[7,8] with modifications. Fasting plasma (1 mL) or AT conditioned media were concentrated by using 100 kDa centrifuge filters (Millipore Amicon Ultra, St. Louis, MO). Concentrated plasma was added to a gel filtration column (Thermo Scientific Disposable 10 mL Polypropelyne Columns, Waltham, MA), packed with a slurry of cross-linked Sepharose CL-2B particles (Sigma-Aldrich), using PBS as the mobile phase. Fractions of 1 mL were eluted by gravity flow and exosome concentration and size in each fraction was determined by Nanoparticle Tracking Analysis (NanoSight, Malvern, Westborough, MA; Camera Level 15, Detection Threshold 5; Supplementary Figure 7*A*). Fractions containing the highest number of exosomes with reduced total concentration of contaminating proteins, determined using dendritic cell (DC) protein assay (Bio-Rad), were collected and further concentrated using 100 kDa centrifuge filters. The purity of the samples was confirmed using immunoblotting for presence of exosome markers (CD63, Cav1, Syntenin, Alix, and HSP90) and absence of other organelle markers (Calnexin for the endoplasmic reticulum [ER], Lamin A/C for the nuclei, and VDAC for the mitochondria) (Supplementary Figures 7*B*, 7*C*, and 7*D*), demonstrating robust isolation of exosomes with minimal contamination by proteins from other organelles. In addition, plasma-derived exosomes contained markers of adipose tissue exosomes (ATGL and Plin-1) (Supplementary Figure 7*D*).

Insulin signal transduction in human skeletal muscle myotubes and mouse hepatocytes. Human skeletal muscle myocytes (Lonza) were induced to differentiate to myotubes per the vendor's instructions. Fully differentiated myotubes were incubated with exosomes (1 x 10^8 particles/mL) for 48 hours. Myotubes were then serum-starved and treated with or without 100 nmol/L insulin. After 15 minutes cells were lysed in ice-cold buffer (20 mmol/L Tris-HCL [pH 7.5], 150 mmol/L NaCL, 1% Triton X-100, 60 mmol/L octyl β-d-glucopyranoside, 200 μmol/L sodium orthovanadate, 50 mmol/L NaF, 1 mmol/L phenylmethylsulfonyl fluoride, and 1.0 μg/mL protease inhibitor mix) and cleared lysates (10,000*g* for 10 minutes) assayed for protein content using DC protein assay (Bio-Rad). Lysates (10 μg protein/lane) were resolved using sodium dodecyl sulfate polyacrylamide gel electrophoresis and analyzed using immunoblotting using antibodies from Cell Signaling Technology for phosphorylated AKT (pAKT Serine 473, Catalog number 4060) and total AKT protein (Catalog number 4691).[9]

Primary hepatocytes were isolated from 8- to 10-week-old C57BL/6 mice as described previously.[10] Mice were infused with a calcium- and magnesium-free Hank's balance salt solution containing 0.5 mmol/L ethylene glycol tetraacetic acid via the inferior vena cava, followed by infusion with 1 mg/mL of type IV collagenase (Sigma Aldrich, catalog number C5138) dissolved in serum-free Dulbecco's modified Eagle medium (DMEM) supplemented with 1 mmol/L pyruvate. After the appearance of cracking on the surface of the liver, the perfusion was stopped immediately and the liver was excised and cells from digested livers were teased out, suspended in DMEM containing 10% fetal bovine serum and antibiotics, filtered through a 100-mm cell strainer, and washed 3 times using centrifugation at 50*g* for 5 minutes at 4°C. After the final wash, the hepatocyte pellet was resuspended in DMEM containing 10% fetal bovine serum and antibiotics and cultured on collagen-coated plates at 37°C under 5% CO_2. After 1 hour of attachment, culture medium was refreshed and exosomes (1 x 10^8 particles/ mL) were added for 48 hours. Hepatocytes were then serum-starved and treated with or without 100 nmol/L insulin. After 15 minutes the cells were lysed, and the lysates were resolved using sodium dodecyl sulfate polyacrylamide gel electrophoresis and were analyzed using immunoblotting, as described for myotubes.

Supplementary References

1. Mifflin MD, St Jeor ST, Hill LA, et al. A new predictive equation for resting energy expenditure in healthy individuals. Am J Clin Nutr 1990;51:241–247.
2. Klein S, Fontana L, Young VL, et al. Absence of an effect of liposuction on insulin action and risk factors for coronary heart disease. N Engl J Med 2004;350:2549–2557.
3. Mittendorfer B, Horowitz JF, Klein S. Gender differences in lipid and glucose kinetics during short-term fasting. Am J Physiol Endocrinol Metab 2001;281:E1333–E1339.
4. Korenblat KM, Fabbrini E, Mohammed BS, et al. Liver, muscle, and adipose tissue insulin action is directly related to intrahepatic triglyceride content in obese subjects. Gastroenterology 2008;134:1369–1375.
5. Yamaguchi S, Franczyk MP, Chondronikola M, et al. Adipose tissue NAD(+) biosynthesis is required for regulating adaptive thermogenesis and whole-body energy homeostasis in mice. Proc Natl Acad Sci U S A 2019;116:23822–23828.
6. **Zunder ER, Finck R,** Behbehani GK, et al. Palladium-based mass tag cell barcoding with a doublet-filtering scheme and single-cell deconvolution algorithm. Nat Protoc 2015;10:316–333.
7. **Flaherty SE 3rd, Grijalva A,** Xu X, et al. A lipase-independent pathway of lipid release and immune modulation by adipocytes. Science 2019;363:989–993.
8. Kreimer S, Ivanov AR. Rapid isolation of extracellular vesicles from blood plasma with size-exclusion chromatography followed by mass spectrometry-based proteomic profiling. Methods Mol Biol 2017;1660:295–302.
9. Samovski D, Dhule P, Pietka T, et al. Regulation of insulin receptor pathway and glucose metabolism by CD36 signaling. Diabetes 2018;67:1272–1284.
10. **McCommis KS, Chen Z,** Fu X, et al. Loss of mitochondrial pyruvate carrier 2 in the liver leads to defects in gluconeogenesis and compensation via pyruvate-alanine cycling. Cell Metab 2015;22:682–694.

Author names in bold designate shared co-first authorship.

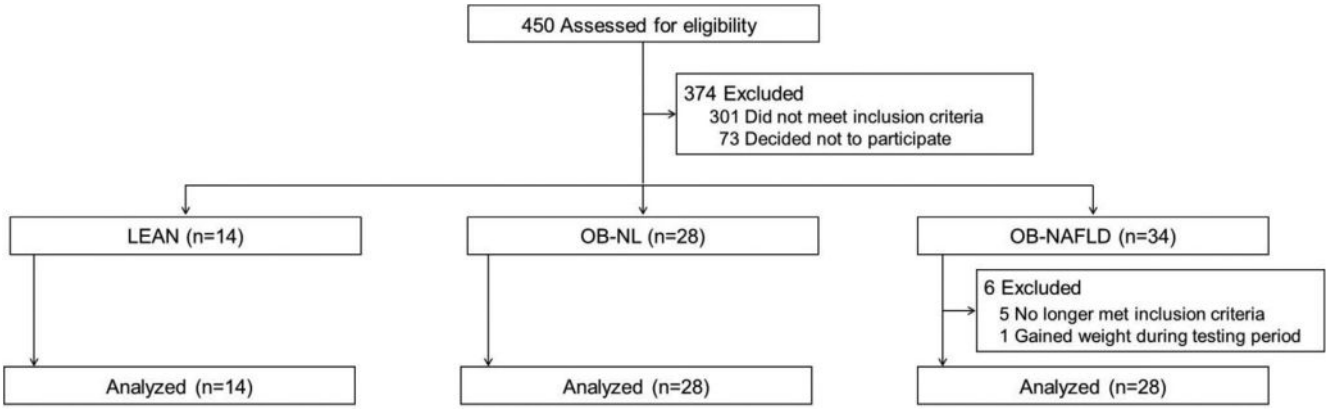

Supplementary Figure 1. Subject flow.

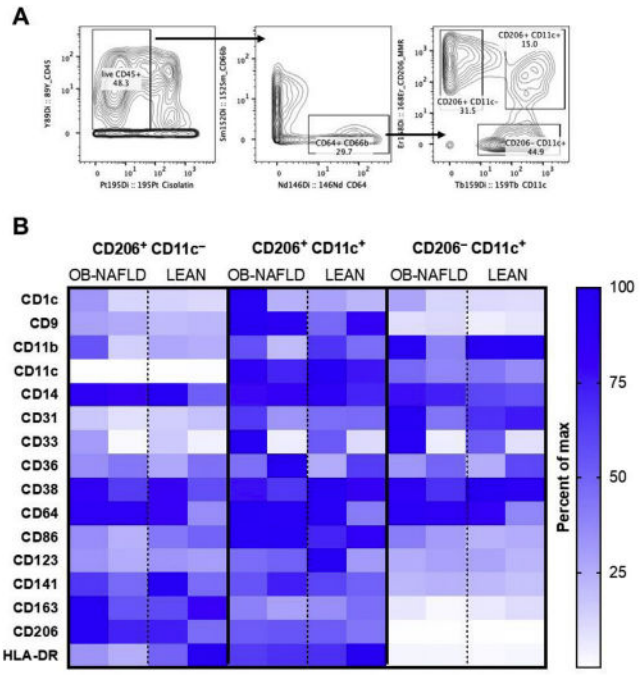

Supplementary Figure 2. Characterization of ATM-related populations within SAAT in 2 people who were OB-NAFLD and 2 people who were lean, analyzed using mass cytometry. (*A*) Macrophages were gated as live CD45$^+$ CD64$^+$ CD66b- cells. Three populations were identified: CD206$^+$ CD11c-, CD206$^+$ CD11c$^+$, and CD206- CD11c$^+$, which were further analyzed for levels of surface marker expression (*B*). (*B*) Heat map of surface markers (each column represents 1 subject) that were detected on either all or a subset of macrophages and their relative expression on individual macrophage subsets (*blue shading* = expression levels relative to row maximum; *dark blue* = maximum expression). Based on this analysis, we classified SAAT macrophages into 2 subsets: (1) CD206$^+$ CD11c$^-$ macrophages; and (2) CD206$^+$ CD11c$^+$ macrophages. A third subset of CD64-positive cells was also identified, but those cells were not categorized as macrophages because they either did not express or expressed very low levels of markers that are characteristic of macrophage subsets (CD206, HLA-DR, CD9, and CD163).

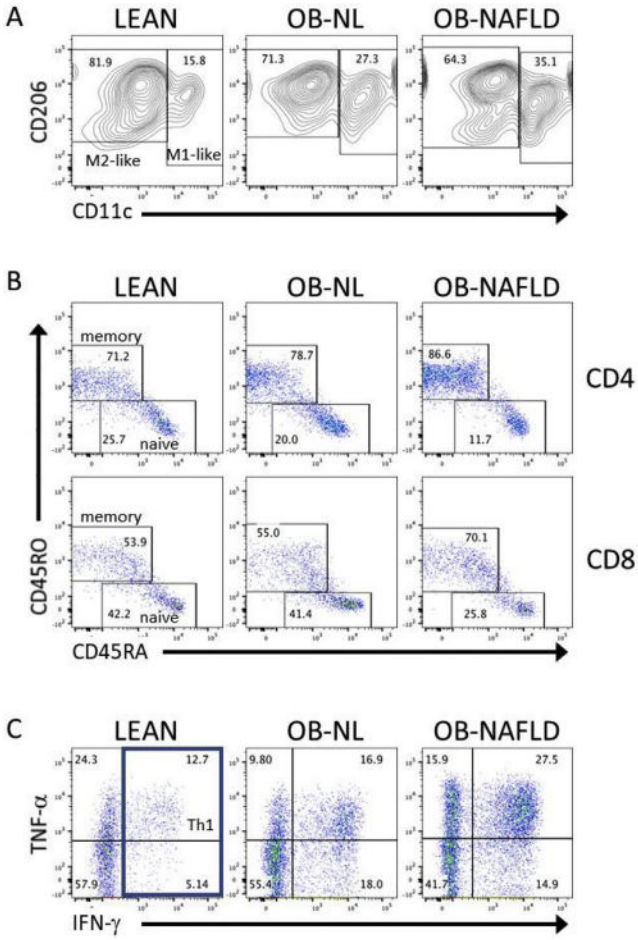

Supplementary Figure 3. Representative flow cytometric analysis of macrophages, naïve and memory T cells, and Th1 cells within the SVF isolated from SAAT from a LEAN, an OB-NL, and an OB-NAFLD subject. (*A*) M1-like (CD11c^{hi}) and M2-like (CD11c^{lo}) macrophages, after gating on CD206+ HLA-DR+ cells. (*B*) Naïve (CD45RA$^+$ CD45RO$^-$) and memory (CD45RA$^-$ CD45RO$^+$) CD4 (*top*) and CD8 (*bottom*) T cells, after gating on CD3+ CD4+ and CD3+ CD8+ cells, respectively. (*C*) IFN-γ–producing Th1 cells, after gating on CD3+ CD4+ cells, after a 5-h culture of SVF with PMA and ionomycin. Numbers in gates and quadrants indicate the frequency of the respective subset within the cell population.

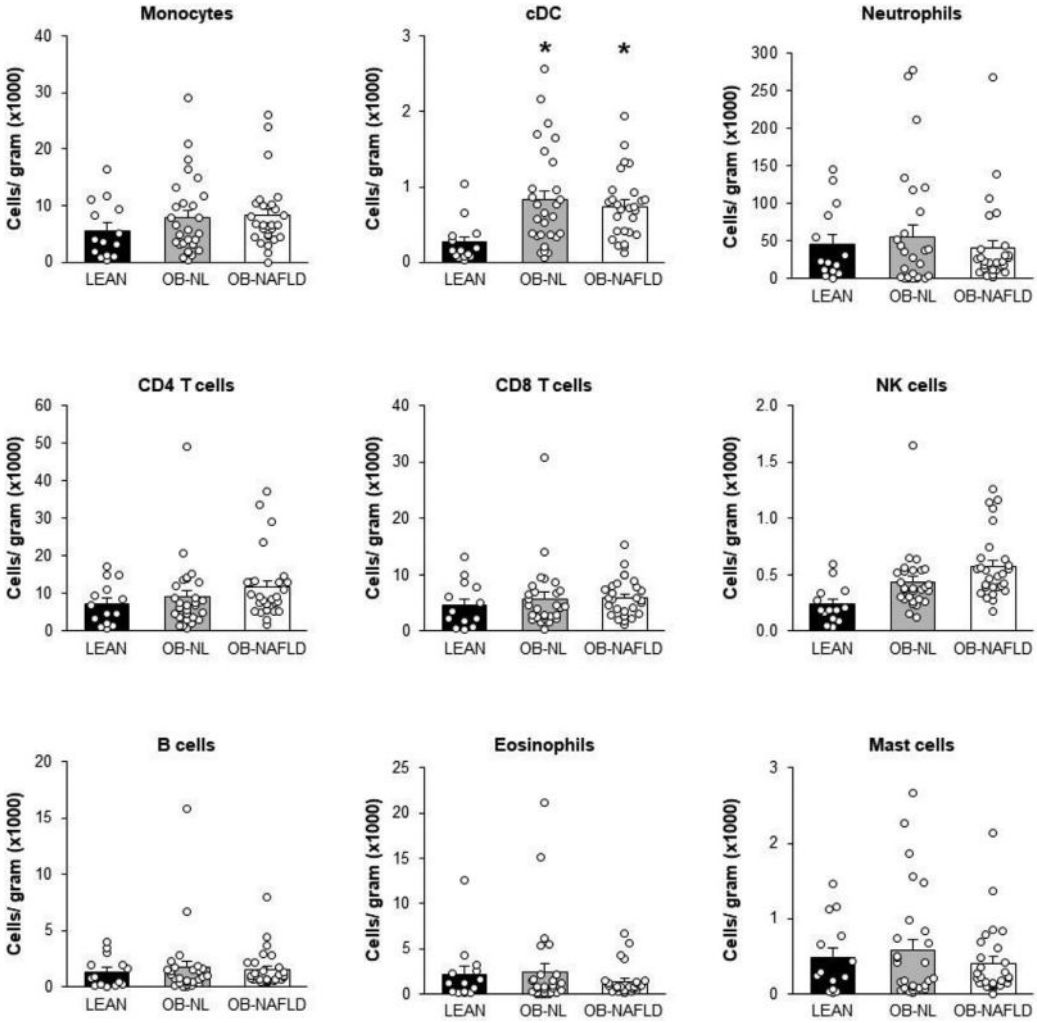

Supplementary Figure 4. Immune cell numbers per gram of SAAT from LEAN, OB-NL, and OB-NAFLD subjects. *Value significantly different from the LEAN value; $P < .05$.

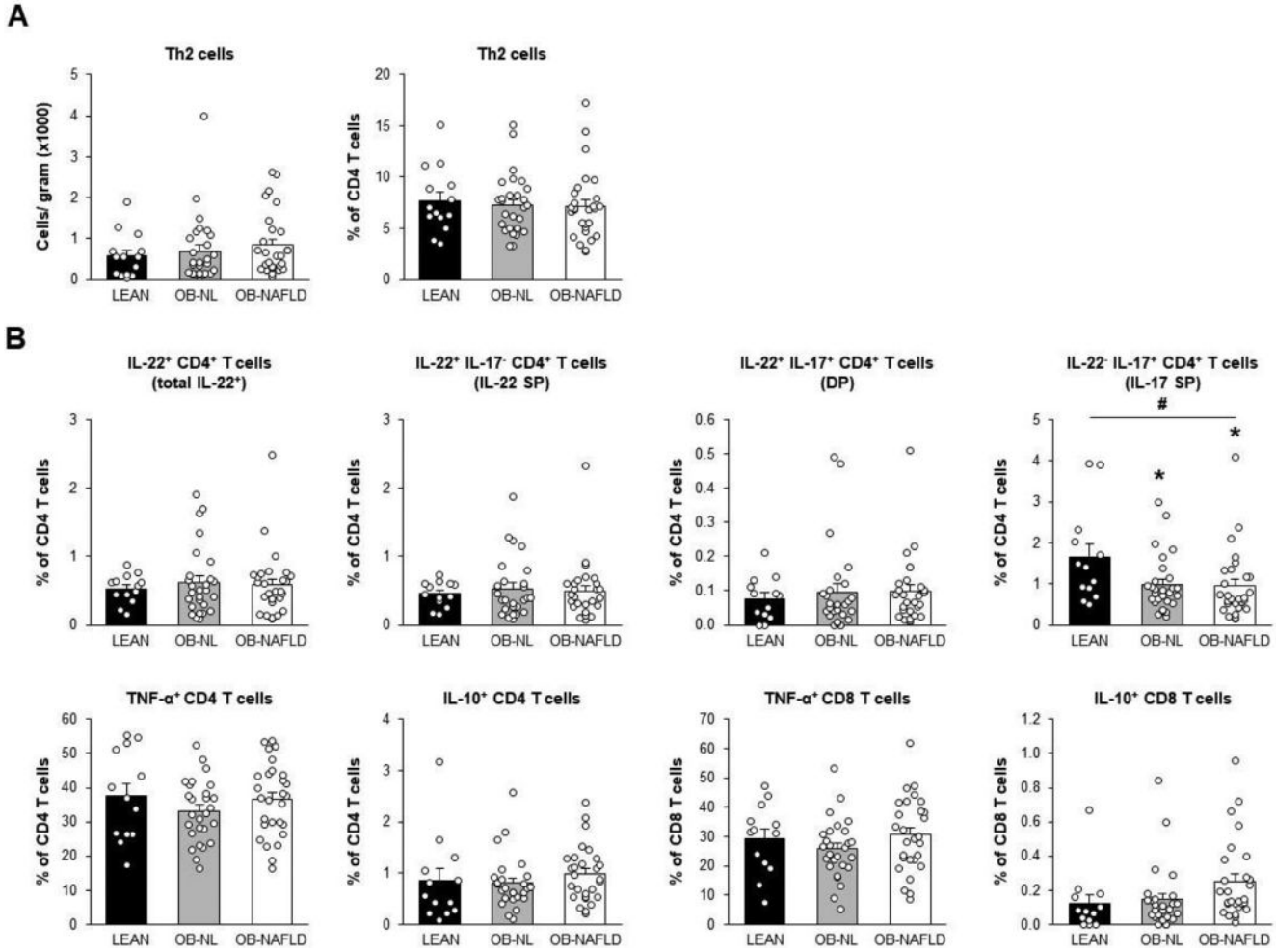

Supplementary Figure 5. (*A*) Absolute number and proportion of Th2 cells. (*B*) Percentage of total IL22-positive, IL22 single positive (SP), IL22 and IL17 double-positive (DP), IL17 SP, TNF-α–positive and IL10-positive CD4 T cells and TNF-α–positive and IL10-positive CD8 T cells following 5-h in vitro stimulation with phorbol ester and ionomycin in SAAT from LEAN, OB-NL, and OB-NAFLD subjects. Values are mean ± SEM. *Value significantly different from the LEAN value; $P < .05$. #Linear trend; $P < .05$.

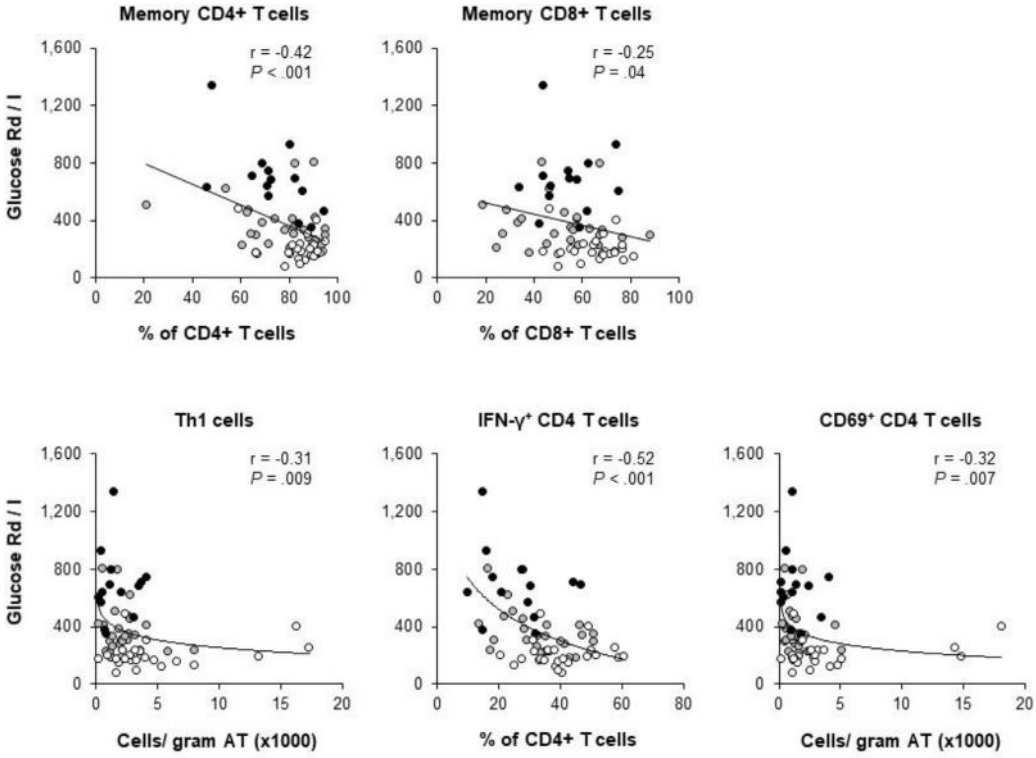

Supplementary Figure 6. Relationship between skeletal muscle insulin sensitivity, assessed as glucose rate of disposal (Rd, in nmol/kg fat-free mass/min) divided by plasma insulin (I) concentration (in μU/mL) during a hyperinsulinemic-euglycemic clamp procedure, and selected proinflammatory T-cell subsets in LEAN (*black circles*), OB-NL (*grey circles*), and OB-NAFLD (*white circles*) participants.

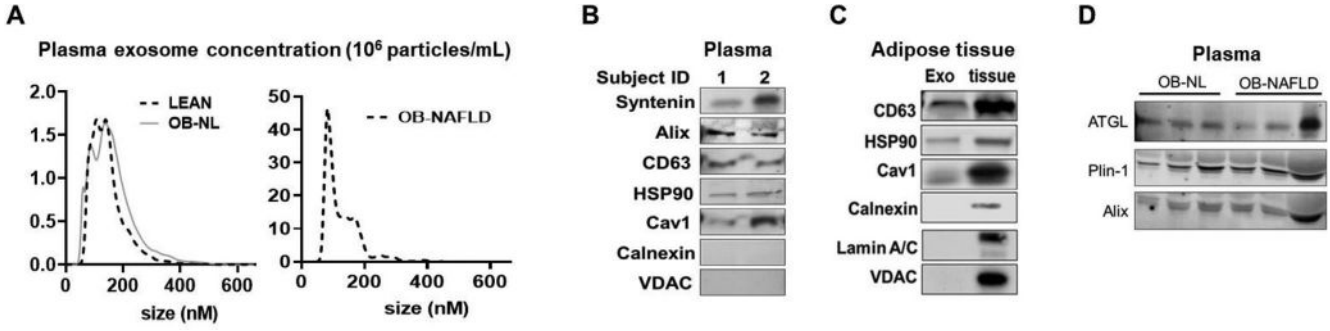

Supplementary Figure 7. Characterization of exosomes isolated from plasma and SAAT. (*A*) Mean particle count and size distribution of plasma exosomes isolated from LEAN (n = 9), OB-NL (n = 8), and OB-NAFLD (n = 7) participants (error bars omitted for clarity). (*B*) Representative immunoblots demonstrating presence of markers of plasma exosomes (Syntenin, Alix, CD63, HSP90, Caveolin1 [Cav1]) and absence of markers of other organelles (Calnexin for the ER and VDAC for the mitochondria) in plasma samples of 2 subjects. (*C*) Representative immunoblots demonstrating presence of markers of AT exosomes (Exo) (CD63, HSP90, and Cav1) and absence of markers of other organelles (Calnexin for the ER, Lamin A/C for the nuclei, and VDAC for the mitochondria) in AT-derived exosomes and presence of all markers in AT lysate, obtained from a subcutaneous abdominal AT explant culture from 1 subject. (*D*) Representative immunoblots demonstrating presence of AT markers (ATGL and Perilipin-1 [Plin-1]) and Alix, a general exosome marker, in plasma-derived samples from 3 OB-NL and 3 OB-NAFLD subjects.

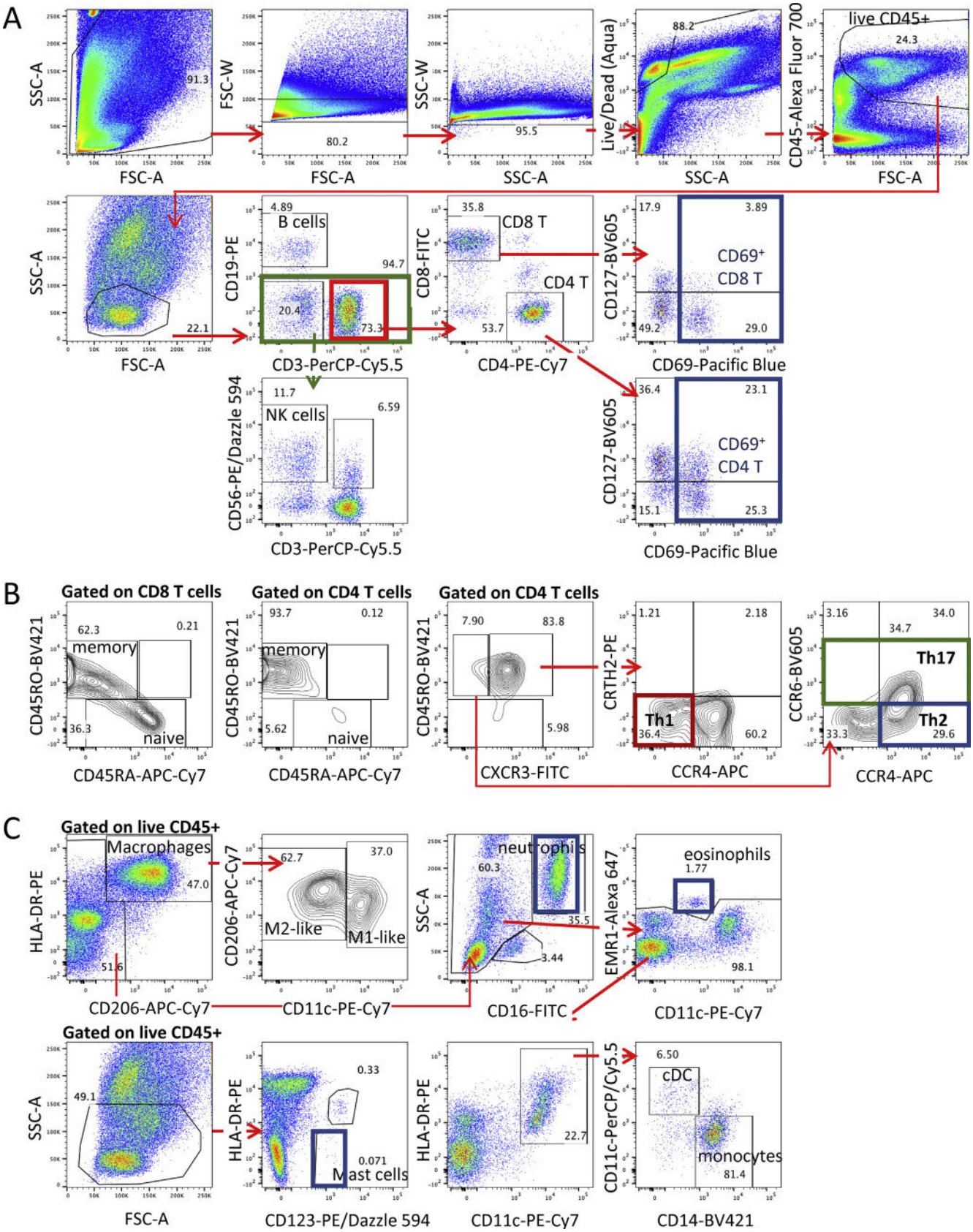

Supplementary Figure 8. Gating strategy for analysis of immune cells using flow cytometry within the SVF isolated from SAAT. (*A*) Gating for individual lymphocyte populations and their expression of CD69. (*B*) Gating strategy for naive and memory CD4 and CD8 T cells. (*C*) Gating strategy for macrophages, neutrophils, eosinophils, monocytes, classical dendritic cell (cDC), and mast cells.

Supplementary Table 1. Body Composition and Metabolic Characteristics of Participants Included in the Plasma Exosome Analysis

	LEAN (n = 9)	OB-NL (n = 8)	OB-NAFLD (n = 7)
Age (*y*)	36 ± 3	39 ± 3	38 ± 4
BMI (kg/m^2)	22.8 ± 0.5	36.2 ± 1.2[a]	41.8 ± 1.6[a,b]
Body fat (%)	29.8 ± 1.9	49.2 ± 1.8[a]	50.0 ± 1.8[a]
IHTG content (%)	1.7 ± 0.2	2.5 ± 0.3 [a]	25.4 ± 2.6[a,b]
IAAT volume (cm^3)	420 ± 70	837 ± 90[a]	2686 ± 282[a,b]
SAAT volume (cm^3)	937 ± 129	3462 ± 314[a]	4132 ± 562[a]
Alanine aminotransferase (*U/L*)	14 ± 2	16 ± 1	64 ± 26[a]
Aspartate aminotransferase (*U/L*)	15 ± 2	16 ± 1	38 ± 11[a,b]
Fasting triglyceride (*mg/dL*)	60 ± 5	60 ± 5	151 ± 17[a,b]
HbA1c (%)	5.0 ± 0.1	5.0 ± 0.1	5.7 ± 0.2[a,b]
Fasting insulin (*μU/mL*)	4.6 ± 0.4	7.7 ± 0.6[a]	37.1 ± 7.2[a,b]
Fasting glucose (*mg/dL*)	86 ± 2	87 ± 1	100 ± 5[a,b]
Glucose at 2 h of OGTT (*mg/dL*)	97 ± 7	108 ± 5	174 ± 7[a,b]
HISI (*1000/[μmol/kg FFM/min] x [μU/mL]*)	11.7 ± 1.1	7.3 ± 0.4[a]	2.0 ± 0.2[a,b]
Glucose Rd/insulin (*nmol/kg FFM/min)/(μU/mL*)	798 ± 74	530 ± 71[a]	142 ± 16[a,b]

NOTE. Data are expressed as mean ± SEM.
[a]$P \leq .05$ value significantly different from the corresponding value in the LEAN group.
[b]$P \leq .05$ value significantly different from the corresponding value in the OB-NL group.

Supplementary Table 2. Body Composition and Metabolic Characteristics of Participants Included in the SAAT Exosome Analysis

	OB-NL (n = 9)	OB-NAFLD (n = 6)	*P* value
Age (*y*)	43 ± 3	46 ± 4	.64
BMI (kg/m^2)	40.1 ± 2.4	43.5 ± 4.7	.49
Body fat (%)	47.7 ± 2.6	46.3 ± 1.8	.70
IHTG content (%)	2.6 ± 0.4	18.0 ± 3.6	<.01
Alanine aminotransferase (*U/L*)	18 ± 2	21 ± 2	.29
Aspartate aminotransferase (*U/L*)	18 ± 1	19 ± 1	.69
Fasting TG (*mg/dL*)	83 ± 9	210 ± 55	.01
HbA1c (%)	5.3 ± 0.1	5.8 ± 0.2	.02
Fasting insulin (*μU/mL*)	12.9 ± 1.8	25.6 ± 5.9	.03
Fasting glucose (*mg/dL*)	88 ± 1	103 ± 2	<.01
Glucose at 2 h of OGTT (*mg/dL*)	110 ± 5	173 ± 7	<.01
HISI (*1000/[μmol/kg FFM/min] x [μU/mL]*)	5.7 ± 0.9	3.4 ± 0.7	.09
Glucose Rd/insulin (*nmol/kg FFM/min)/(μU/mL*)	441 ± 42	229 ± 37	<.01

NOTE. Data are expressed as mean ± SEM.

Supplementary Table 3. Antibodies Used for Mass Cytometric Macrophage Analysis

Label	Target	Clone	Manufacturer
089Y	CD45	HI30	Fluidigm
145Nd	CD31	WM59	Fluidigm
146Nd	CD64	10.1	Fluidigm
151Eu	CD123	6H6	Fluidigm
154Sm	CD163	GHI/61	Fluidigm
155Gd	CD36	5-271	Fluidigm
156Gd	CD86	IT2.2	Fluidigm
159Tb	CD11c	Bu15	Fluidigm
160Gd	CD14	M5E2	Fluidigm
165Ho	CD16	3G8	Fluidigm
166Er	CD141	M80	Fluidigm
167Er	CD38	HIT2	Fluidigm
168Er	CD206 (MMR)	15-2	Fluidigm
169Tm	CD1c	L161	Biolegend, Immunomonitoring Laboratory
171Yb	CD9	SN4 C3-3A2	Fluidigm
173Yb	CD33	P67.6	BD, Immunomonitoring Laboratory
174Yb	HLA-DR	L243	Fluidigm
209Bi	CD11b	ICRF44	Fluidigm

Supplementary Table 4. Antibodies Used for Flow Cytometric Immune Cell Analysis

Antibody	Source	Identifier (catalog number)
Panel 1: myeloid cells		
CD45-Alexa700, clone HI30	Biolegend	304024
HLA-DR-PE, clone L243	Biolegend	307606
CD14-Brilliant Violet 421, clone HCD14	Biolegend	325628
CD16-FITC, clone 3G8	Biolegend	302006
CD206-APC/Cy7, clone 15-2	Biolegend	321119
CD11c-PE/Cy7, clone Bu15	Biolegend	337216
CD1c-PerCP/Cy5.5, clone L161	Biolegend	331514
EMR1-Alexa Fluor 647, clone A10	Bio-Rad (Serotec)	MCA2674A647
CD86-Brilliant Violet 605, clone IT2.2	Biolegend	305430
CD123-PE/Dazzle 594, clone 6H6	Biolegend	306034
Zombie-Aqua fixable live/dead dye	Biolegend	423101
Panel 2: lymphocytes		
CD45-Alexa700, clone HI30	Biolegend	304024
CD3-PerCP/Cy5.5, clone HIT3a	Biolegend	300328
CD4-PE/Cy7, clone OKT4	Biolegend	317414
CD8-FITC, clone HIT8a	Biolegend	300906
CD56-PE/Dazzle 594, clone HCD56	Biolegend	318348
CD69-Pacific Blue, clone FN50	Biolegend	310920
CD19-PE, clone HIB19	Biolegend	302208
HLA-DR-APC/Fire 750, clone L243	Biolegend	307658
Zombie-Aqua fixable live/dead dye	Biolegend	423101
Panel 3: memory/naive T cells, Th1/2/17 cells		
CD45-Alexa700, clone HI30	Biolegend	304024
CD3-PerCP/Cy5.5, clone HIT3a	Biolegend	300328
CD4-PE/Cy7, clone OKT4	Biolegend	317414
CD8-PE/Dazzle 594, clone RPA-T8	Biolegend	301057
CRTH2-PE, clone BM16	Biolegend	350106
CXCR3-FITC, clone G025H7	Biolegend	353704
CCR4-APC, clone L291H4	Biolegend	359408
CCR6-Brilliant Violet 605, clone G034E3	Biolegend	353420
CD45RA-APC/Cy7, clone HI100	Biolegend	304127
CD45RO-Brilliant Violet 421, clone UCHL1	Biolegend	304224
Zombie-Aqua fixable live/dead dye	Biolegend	423101
Panel 4: intracellular cytokine staining		
CD45-Alexa700, clone HI30	Biolegend	304024
CD3-PerCP/Cy5.5, clone HIT3a	Biolegend	300328
CD4-PE/Cy7, clone OKT4	Biolegend	317414
CD8-FITC, clone HIT8a	Biolegend	300906
CD56-PE/Dazzle 594, clone HCD56	Biolegend	318348
IFN-γ-Brilliant Violet 421, clone 4S.B3	Biolegend	502532
TNF-α-APC/Cy7, clone Mab11	Biolegend	502944
IL22-PE, clone BG/IL22 (replacement: clone 22URTI)	Biolegend, eBioscience	515303 12-7229-42
IL17A-Brilliant Violet 605, clone BL168	Biolegend	512326
IL10-Alexa Fluor 647, clone JES3-9D7	Biolegend	501412
Zombie-Aqua fixable live/dead dye	Biolegend	423101

Supplementary Table 5. Gating Strategy for Flow Cytometric Immune Cell Analysis

Subset	Surface markers used for identification
B cells	SSC^{lo} $CD3^{-}$ $CD19^{+}$
CD4 T cells	SSC^{lo} $CD19^{-}$ $CD3^{+}$ $CD4^{+}$ $CD8^{-}$
CD8 T cells	SSC^{lo} $CD19^{-}$ $CD3^{+}$ $CD4^{-}$ $CD8^{+}$
NK cells	SSC^{lo} $CD19^{-}$ $CD3^{-}$ $CD56^{+}$
Naïve CD4 T cells	SSC^{lo} $CD3^{+}$ $CD4^{+}$ $CD8^{-}$ $CD45RA^{+}$ $CD45RO^{-}$
Memory CD4 T cells	SSC^{lo} $CD3^{+}$ $CD4^{+}$ $CD8^{-}$ $CD45RA^{-}$ $CD45RO^{+}$
Naïve CD8 T cells	SSC^{lo} $CD3^{+}$ $CD4^{-}$ $CD8^{+}$ $CD45RA^{+}$ $CD45RO^{-}$
Memory CD8 T cells	SSC^{lo} $CD3^{+}$ $CD4^{-}$ $CD8^{+}$ $CD45RA^{-}$ $CD45RO^{+}$
Th1 cells	SSC^{lo} $CD3^{+}$ $CD4^{+}$ $CD8^{-}$ $CD45RO^{+}$ $CXCR3^{+}$ $CCR4^{-}$ $CCR6^{-}$
Th2 cells	SSC^{lo} $CD3^{+}$ $CD4^{+}$ $CD8^{-}$ $CD45RO^{+}$ $CXCR3^{-}$ $CCR4^{+}$ $CCR6^{-}$
Th17 cells	SSC^{lo} $CD3^{+}$ $CD4^{+}$ $CD8^{-}$ $CD45RO^{+}$ $CXCR3^{-}$ $CCR4^{-/+}$ $CCR6^{+}$
Mast cells	$CD123^{+}$ HLA-DR^{-}
Macrophages	$CD206^{+}$ HLA-DR^{+}
M1-like macrophages	$CD206^{+}$ HLA-DR^{+} $CD11c^{hi}$
M2-like macrophages	$CD206^{+}$ HLA-DR^{+} $CD11c^{lo}$
Neutrophils	$CD206^{-}$ $CD16^{hi}$ SSC^{hi}
Eosinophils	$CD206^{-}$ $CD16^{-/lo}$ $EMR1^{+}$
Monocytes	$CD206^{-}$ HLA-DR^{+} $CD11c^{+}$ $CD14^{+}$ $CD1c^{-}$
Classical (myeloid) DCs	$CD206^{-}$ HLA-DR^{+} $CD11c^{+}$ $CD14^{-}$ $CD1c^{+}$

NOTE. Cells were initially gated on live ($Aqua^{-}$), single (FSC-area vs -width and SSC-area vs. -width), $CD45^{+}$ cells.
FSC, forward scatter; SSC, side scatter.